ZADÁNÍ DIPLOMOVÉ PRÁCE

I. OSOBNÍ A STUDIJNÍ ÚDAJE

Příjmení: **Mikluš** Jméno: **Michal** Osobní číslo: **475079**

Fakulta/ústav: **Fakulta strojní**

Zadávající katedra/ústav: **Ústav technické matematiky**

Studijní program: **Aplikované vědy ve strojním inženýrství**

Specializace: **Matematické modelování v technice**

II. ÚDAJE K DIPLOMOVÉ PRÁCI

Název diplomové práce:

Úpravy RANS modelu turbulence pro prudění v blízkosti stěny

Název diplomové práce anglicky:

Modifications of RANS turbulence model for wall bounded flows

Pokyny pro vypracování:

Student
1) se seznámí s modelem k-epsilon-v2-f a k-epsilon-phit-f popíše rozdíly mezi nimi
2) provede simulace proudění pro vybrané případy
3) popíše známé modifikace modelu
4) navrhne vlastní modifikaci pro specifický případ proudění

Seznam doporučené literatury:

[1] Wilcox: Turbulence Modeling for CFD, ISBN 1928729088
[2] Durbin: Statistical Theory and Modeling for Turbulent Flows, ISBN 9780470689318
[3] Louda, Příhoda: Modelování turbulence, skripta FS ČVUT

Jméno a pracoviště vedoucí(ho) diplomové práce:

prof. Ing. Jiří Fürst, Ph.D. ústav technické matematiky FS

Jméno a pracoviště druhé(ho) vedoucí(ho) nebo konzultanta(ky) diplomové práce:

Datum zadání diplomové práce: **12.04.2023** Termín odevzdání diplomové práce: **13.08.2023**

Platnost zadání diplomové práce: _____

prof. Ing. Jiří Fürst, Ph.D. podpis vedoucí(ho) práce	prof. Ing. Jiří Fürst, Ph.D. podpis vedoucí(ho) ústavu/katedry	doc. Ing. Miroslav Španiel, CSc. podpis děkana(ky)

III. PŘEVZETÍ ZADÁNÍ

Diplomant bere na vědomí, že je povinen vypracovat diplomovou práci samostatně, bez cizí pomoci, s výjimkou poskytnutých konzultací. Seznam použité literatury, jiných pramenů a jmen konzultantů je třeba uvést v diplomové práci.

. _____ _____

Datum převzetí zadání Podpis studenta

FACULTY
OF MECHANICAL
ENGINEERING
CTU IN PRAGUE

Master's thesis

Modifications of RANS turbulence model for wall bounded flows

Bc. Michal Mikluš

Department of Technical Mathematics
Supervisor: prof. Ing. Jiří Fürst, Ph.D.

July 24, 2023

Acknowledgements

I would like to thank my family and friends for their support during writing this thesis.

Declaration

I hereby declare that the presented thesis is my own work and that I have cited all sources of information in accordance with the Guideline for adhering to ethical principles when elaborating an academic final thesis.

I acknowledge that my thesis is subject to the rights and obligations stipulated by the Act No. 121/2000 Coll., the Copyright Act, as amended. In accordance with Article 46 (6) of the Act, I hereby grant a nonexclusive authorization (license) to utilize this thesis, including any and all computer programs incorporated therein or attached thereto and all corresponding documentation (hereinafter collectively referred to as the "Work"), to any and all persons that wish to utilize the Work. Such persons are entitled to use the Work for nonprofit purposes only, in any way that does not detract from its value. This authorization is not limited in terms of time, location and quantity.

In Prague on July 24, 2023 . . . . . .

Czech Technical University in Prague
Faculty of Mechanical Engineering

Citation of this thesis

Mikluš, Michal. *Modifications of RANS turbulence model for wall bounded flows.* Master's thesis. Czech Technical University in Prague, Faculty of Mechanical Engineering, 2023.

Abstrakt

Jedním z cílů diplomové práce je seznámit se s třídou modelů s vířivou viskozitou rozšířených o eliptickou relaxaci, zvanou $\overline{v^2} - f$ modely. Pro výpočet dvou případů práce je vybrána dostatečně robustní formulace $\varphi - f$. Budou zavedeny různé modifikace, diskutováno jejich teoretické pozadí a nakonec budou aplikovány na model $\varphi - f$, s cílem zlepšení předpovědí přenosu tepla pro impaktní proudení. Jsou uvažovány dvě konfigurace impaktního proudení - jedna, kde mezní vrstva prochází laminárním - turbulentním přechodem a druhá, kde je mezní vrstva všude turbulentní. Modifikace jsou primárně navrženy tak, aby zabránily hromadění turbulentní kinetické energie v stagnačních oblastech. U některých z úprav budou také validovány profily rychlosti a smykového napětí. Nejobecnější modifikace, podmínka realizovatelnosti, bude použita také v konfiguraci průtoku tvořené dvěma 180° U-ohyby. Její účinek na předpovědi rychlostních profilů a distribuce třecích koeficientu bude analyzován. Některé podrobnosti o implementaci podmínky realizovatelnosti budou zdůrazněny. Celková diskuse je v tomto ohledu rozšířena také na modely $k - \omega$.

Klíčová slova RANS modelování, dvourovnicové modely s turbulentní viskozitou, eliptická relaxace, podmínka realizovatelnosti, stagnační anomálie

Abstract

One of the thesis' goals is to get acquainted with a class of linear eddy viscosity models augmented with elliptic relaxation, called $\overline{v^2} - f$ models. A sufficiently robust formulation, $\varphi - f$, is selected to compute the thesis' two cases. Various modifications will be introduced, their theoretical background discussed, and finally applied to the $\varphi - f$ model to improve heat transfer predictions in the impinging jet case. Two nozzle-to-plate spacings are considered - one where a boundary layer undergoes a laminar-turbulent transition and the other where the boundary layer is fully turbulent everywhere. The considered modifications are primarily designed to prevent the build-up of turbulence kinetic energy in stagnation regions. Some of the modifications will be also validated against the experimental data of mean velocity and Reynolds shear stress profiles. The most general one, the realizability constraint, will be also applied in a flow configuration made up of two 180° U-bends. Its effect on predictions of mean velocity profiles and skin friction coefficient distributions will be analyzed and possible consequences will be discussed. Some subtle details about the implementation of the realizability constraints will be pointed out. The overall discussion is in this regard extended to the $k - \omega$ models as well.

Keywords RANS modeling, two-equation eddy viscosity models, elliptic relaxation, realizability constraint, stagnation anomaly

Contents

List of Figures

List of Tables

List of symbols

Θ	Thermodynamic temperature. (K)
β_T	Clauser's pressure gradient parameter, defined as $\frac{\delta_*}{\tau_w}\frac{\mathrm{d}P_o}{\mathrm{d}x}$, where δ^* is displacement thickness, τ_w is wall shear stress and P_o is free stream pressure. A boundary layer is formally in equilibrium if β_T is constant downstream. (1)
δ_{ij}	Kronecker delta symbol. $\delta_{ij} = 1$ when $i = j$, otherwise it equals zero. It can also refer to an isotropic second-rank tensor.
$\lvert\Omega\rvert$	Magnitude of vorticity tensor, $\lvert\Omega\rvert = \sqrt{\Omega_{ij}\Omega_{ij}}$. ($\mathrm{s}^{-1}$)
$\lvert S\rvert$	Magnitude of strain-rate, $\lvert S\rvert = \sqrt{S_{ij}S_{ij}}$. ($\mathrm{s}^{-1}$)
$\mathcal{P}_k$	Production rate of kinetic energy k. ($\mathrm{m}^2\mathrm{s}^{-3}$)
ν	Kinematic viscosity. ($\mathrm{m}^2\,\mathrm{s}^{-1}$)
ν_T	Eddy viscosity. ($\mathrm{m}^2\,\mathrm{s}^{-1}$)
ω	Specific dissipation frequency. (s^{-1})
Ω_{ij}	Components of the skew-symmetric part of the velocity gradient $\frac{1}{2}\left(\frac{\partial U_i}{\partial x_j} - \frac{\partial U_j}{\partial x_i}\right)$, called vorticity tensor. (s^{-1})
$\overline{u_i u_j}$	Components of the Reynolds stress tensor. ($\mathrm{m}^2\,\mathrm{s}^{-2}$)
$\overline{v^2}$	Covariance of wall normal velocity fluctuations. ($\mathrm{m}^2\mathrm{s}^{-2}$)
ϕ_{ij}	Velocity pressure gradient correlation. ($\mathrm{m}^2\mathrm{s}^{-3}$)
τ_w	Wall shear stress. Due to the incompressibility assumption, density is absorbed into to the wall shear stress. ($\mathrm{m}^2\mathrm{s}^{-2}$)
$\frac{\mathrm{D}}{\mathrm{D}t}$	Convective derivative, defined as : $\frac{\partial}{\partial t} + U_j\frac{\partial}{\partial x_j}$.

ε	Specific dissipation rate of kinetic energy k. ($\mathrm{m^2 s^{-3}}$)
ε_{ij}	Dissipation tensor appearing in transport equations for Reynolds stresses. ($\mathrm{m^2 s^{-3}}$)
φ (ζ)	$\overline{v^2}$ normalized by kinetic energy k. (1)
c_f	Skin friction coefficient. (1)
f	Rescaled wall normal component of the redistribution tensor. (1)
k	Specific turbulence kinetic energy $\frac{1}{2}\overline{u_i u_i}$, often referred to simply as kinetic energy or turbulence kinetic energy. ($\mathrm{m^2\,s^{-2}}$)
L	Turbulence length scale, proportional to $\frac{k^{3/2}}{\varepsilon}$. (m)
Nu	Nusselt number. (1)
P	Reynolds averaged kinematic pressure, the density is absorbed due to the incompressibility assumption. ($\mathrm{m^2\,s^{-2}}$)
Pr	Prandtl and turbulent Prandlt number. (1)
Pr_T	Turbulent Prandtl number. (1)
r_i	Components of the normalized velocity vector $U_i/\lvert U\rvert$. (1)
S_{ij}	Components of the symmetric part of the velocity gradient $\frac{1}{2}\left(\frac{\partial U_i}{\partial x_j} + \frac{\partial U_j}{\partial x_i}\right)$, called strain-rate or (mean) rate of strain. ($\mathrm{s^{-1}}$)
T	Turbulence time scale, proportional to $\frac{k}{\varepsilon}$. (s)
U_i	Components of the Reynolds averaged velocity. ($\mathrm{m\,s^{-1}}$)

Introduction

The vast majority of flows occurring in nature and ones of practical interest, are turbulent. Turbulent motion can be at first glance characterized by the chaotic and irregular occurrence of "eddies". Particular realizations of turbulent flow are seemingly random, but at the statistical level, turbulent phenomena are reproducible and can be systematically analyzed. Perhaps the most straightforward approach to tackle the difficult task of describing the turbulent motion is to solve time-dependent, three-dimensional Navier-Stokes equations. The computed chaotic flow field would then be averaged in time to obtain statistics. This approach employs no modeling and is a rather direct one, hence it is called a direct numerical simulation (DNS).

One of the characteristic properties of turbulence is the presence of a continuous, wide range of scales. Big eddies, generated by mean shear carrying large amounts of kinetic energy get grounded down to the smallest possible eddies, which then get dissipated by viscosity. If one wants to correctly compute the statistics of turbulent flows using DNS, one has to capture the whole energy cascade, down to the Kolmogoroff length scale. The number of grid points necessary to capture all length scales of turbulence increases roughly to the 9/4-th power of the Reynolds number. Thus for flows of practical interest, direct numerical simulation is not applicable, the computational cost would be simply too high.

A far more tractable approach consists of trying to compute the desired statistics without access to random flow field realizations. The content of this thesis will be focused on solving stationary Reynolds averaged Navier-Stokes equations for incompressible flows:

$$\frac{\mathrm{D}U_i}{\mathrm{D}t} = -\frac{\partial P}{\partial x_i} + \nu\frac{\partial^2 U_i}{\partial x_j \partial x_j} - \frac{\partial \overline{u_i u_j}}{\partial x_j}. \tag{1}$$

Note that density was absorbed into pressure, so P denotes Reynolds averaged kinematic pressure, with dimensions $\mathrm{m}^2\mathrm{s}^{-2}$. The solution of the mean momentum equation is also subjected to a kinematic constrain, called the continuity

equation:

$$\frac{\partial U_i}{\partial x_i} = 0. \tag{2}$$

The last term of equation (1) denotes a divergence of averaged products of fluctuation velocity components. $-\overline{u_i u_j}$ is a covariance matrix - a symmetric second rank tensor called Reynolds stress tensor. The components of this tensor are also unknown, thus the mean momentum equation is not closed. This closure problem is not solved by deriving a transport equation for the Reynolds stresses, which will inevitably contain third moments. Therefore the components of the Reynolds stress tensor have to be modeled in some fashion.

A popular modeling approach is the eddy viscosity concept, where the Reynolds stresses are determined from a linear stress-strain relation:

$$-\overline{u_i u_j} = 2\nu_T S_{ij} + \frac{2}{3} k \delta_{ij} \tag{3}$$

Eddy viscosity intuitively represents averaged effects of random turbulent convection - enhanced diffusion and momentum transport. S_{ij} denotes the symmetric part of the gradient of mean velocity, which can be readily obtained from the mean momentum equation. Eddy viscosity closures, therefore, recast the problem of determining the Reynolds stresses to determining the scalar eddy viscosity ν_T. The dimensions of eddy viscosity are the same as those of molecular viscosity. A simple dimensional analysis reveals that a valid expression for eddy viscosity could be formed from a product of some squared velocity scale (or energy scale, but the most frequently used term is simply velocity scale) ($\mathrm{m^2 s^{-2}}$) and a time scale (s). A natural velocity scale is turbulence kinetic energy k. Turbulence models considered in this thesis will all involve a transport equation for $k = \frac{1}{2}\overline{u_i u_i}$. This equation can be derived as one-half of the trace Reynolds stress transport equation and can even be straightforwardly closed. We also need to compute a second turbulence quantity to form a dimensionally consistent eddy viscosity, a most natural one is the specific dissipation rate of kinetic energy ε ($\mathrm{m^2 s^{-3}}$), with which we can form a turbulence time scale k/ε. Another turbulence quantity that can be considered is the inverse time-scale ratio, or so-called specific kinetic energy dissipation frequency ω ($\mathrm{s^{-1}}$), where the eddy viscosity is formed as a fraction k/ω. Unfortunately, the transport equation for the dissipation rate can be derived, but cannot be closed as easily as the one for kinetic energy. Thus both transport equations for ε and ω are formed as dimensionally consistent equivalents to the k equation. Consequently, two-equation scale-determining models using ε (ω) are called $k-\varepsilon$ ($k-\omega$) models.

Regardless of the choice of second scale variable, for all linear eddy viscosity closures, the production term is quadratic in symmetric mean velocity gradient magnitude:

$$\mathcal{P}_k = 2\nu_T S_{ij} S_{ij} = 2\nu_T |S|^2. \tag{4}$$

In full second moment closures the production rate of kinetic energy doesn't have to be modeled and is linear in mean velocity gradient:

$$\mathcal{P}_k = -\overline{u_i u_j}\frac{\partial U_i}{\partial x_j} = -\overline{u_i u_j} S_{ij}. \tag{5}$$

The striking difference between the equations (4) and (5) is the cause of the tendency of linear eddy viscosity models to overpredict the turbulence kinetic energy levels whenever the non-shear related strain rate is high. Examples of such flows are inviscid stagnation, and decelerated flow in a diffuser. A great case for studying stagnation point anomalies is normally impinging jet on a flat plate, which will be the main case study of this thesis.

The thesis is divided into four chapters. The first chapter tries to motivate the use of the elliptic relaxation framework in RANS models, in particular, linear eddy viscosity models. The use of turbulence kinetic energy as a velocity scale in near-wall regions is questioned. The second chapter assesses the numerical robustness of several formulations of a $\overline{v^2} - f$ model. These are a class of $k - \varepsilon$ models combined with elliptic relaxation. A sufficiently robust formulation and arguably the most consistent with the original $\overline{v^2} - f$ model, $\varphi - f$, was chosen for the application to the two case studies. The third chapter will be focused on predictions of heat transfer rates in a jet normally impinging jet on a flat plate, where various modifications to the $\varphi - f$ model will be applied to suppress a spurious overproduction of turbulence kinetic energy in stagnation regions. All of the models and subsequent modifications were implemented in a numerical library OpenFOAM. The effectiveness of these modifications will be validated against the experimental data of Baughn et. al [2]. Some of the modifications will get quite a lot of exposition since the motivation behind them is linked to the general theory of two-equation scale-determining models. Guided by the mechanisms of other modifications and exploiting the flow configuration of an impinging jet, the author will attempt to come up with his own modifications, which will serve as heuristic proof of the cause of stagnation anomalies. The fourth chapter will serve as a counterexample to the third, where a flow with pressure-induced separation through two 180° U-bends will be considered. The appropriateness of use of most theoretically sound modifications, the realizability constraints, will be challenged. The predictions will be validated against the DNS data of Durbin et. al [7]. The discussion will be extended to the $k-\omega$ models as well. Limitations surrounding the application of ad hoc modifications to the eddy viscosity models will be discussed in the conclusion.

Chapter 1

Motivation for choosing $\overline{v^2}$ as the velocity scale

To appreciate the importance of $\overline{v^2} - f$ models and elliptic relaxation in full second-moment closure, the $k - \varepsilon$ model has to be introduced and discussed. The "standard" $k - \varepsilon$ model is one of the oldest two-equation models and is widely used even today. Models of $k - \varepsilon$ type are linear eddy viscosity models, all of which employ the following formula for eddy viscosity:

$$\nu_T = C_\mu \frac{k^2}{\varepsilon}, \tag{1.1}$$

and the standard value of C_μ is 0.09. The equation for kinetic energy k reads:

$$\frac{\mathrm{D}k}{\mathrm{D}t} = \mathcal{P}_k - \varepsilon + \frac{\partial}{\partial x_j}\left[\left(\nu + \frac{\nu_T}{\sigma_k}\right)\frac{\partial k}{\partial x_j}\right], \tag{1.2}$$

with the value of $\sigma_k = 1.0$. Equation for specific dissipation rate ε has the following form:

$$\frac{D\varepsilon}{Dt} = \frac{\varepsilon}{k}\left(C_{\varepsilon 1}\mathcal{P}_k - C_{\varepsilon 2}\varepsilon\right) + \frac{\partial}{\partial x_j}\left[\left(\nu + \frac{\nu_T}{\sigma_\varepsilon}\right)\frac{\partial \varepsilon}{\partial x_j}\right]. \tag{1.3}$$

Equation written above is the simplest form of a transport equation, that will produce at least qualitatively correct behavior for ε. It can be interpreted as a dimensionally consistent equivalent of the equation for kinetic energy. Large production rates of turbulence kinetic energy must lead to large dissipation rates. When the production rate vanishes, the dissipation rate shall diminish fast enough to prevent negative energy levels. As is the case of the equation for the kinetic energy, the transport equation also has a source and a sink term proportional to the production and dissipation rate. The standard values of the constants in the equation are the following [8, Sec. 6.2]:

$$C_{\varepsilon 1} = 1.44,\ C_{\varepsilon 2} = 1.92,\ \sigma_\varepsilon = 1.3.$$

The pair of constants $C_{\varepsilon 1}, C_{\varepsilon 2}$ are important. Value of $C_{\varepsilon 2}$ can be related to the decay rate of isotropic turbulence. Value of $C_{\varepsilon 1}$ controls the spreading rate of free shear layers.

Turbulence kinetic energy is by definition $\frac{1}{2}\overline{u_i u_i}$, therefore has a quadratic zero at the wall. This means that k and its derivative in the wall-normal direction vanishes as the wall is approached. The correct boundary conditions for k at the wall are the following:

$$k = 0, \ \frac{\partial k}{\partial x_j} n_j = 0, \tag{1.4}$$

where n_j are the components of the unit wall-normal vector. The fraction $T = k/\varepsilon$ represents a turbulence time-scale and $T = \mathcal{O}(y^2)$ as $y \to 0$. This behavior creates a singularity in the equation for the dissipation rate. Durbin proposed a lower bound on the time-scale ratio:

$$T = \max\left(\frac{k}{\varepsilon}, \ 6\sqrt{\frac{\nu}{\varepsilon}}\right), \tag{1.5}$$

where the lower limit is proportional to Kolmogoroff time scale. Kolmogoroff scaling is more appropriate near walls [9].

In most CFD codes, the boundary condition (1.4) gets split into two. The Dirichlet boundary condition $k = 0$ is imposed, but the second one is imposed through a condition on ε, which comes from a near-wall balance of the kinetic energy equation:

$$\varepsilon = \nu \frac{\partial^2 k}{\partial y^2}. \tag{1.6}$$

Integrating the equation and imposing the conditions (1.4) by setting the integration constants up to a linear term to zero, gives the following asymptotic behavior for k:

$$k \to \varepsilon \frac{y^2}{2\nu} \quad as \quad y \to 0.$$

The boundary value of ε can be computed by evaluating the limiting expression

$$\varepsilon \to \frac{2\nu k}{y^2} \quad as \quad y \to 0 \tag{1.7}$$

at the first computational node above the wall.

This model can be applied to free shear flows and works well for wall-bounded flows in regions far away from the walls. But once the walls are approached, the model breaks down. It turns out that the eddy viscosity formula (1.1) gives an erroneous profile of eddy viscosity even when the exact profiles of k and ε are substituted. The solid line in figure 1.1 is the eddy viscosity constructed from DNS data of turbulent channel flow [1], by invoking the formula: $\nu_T = -\overline{uv}/\mathrm{d}_y U$. Eddy viscosity gets grossly overpredicted in the region $y_+ < 50$, as the dashed line constructed from the $k-\varepsilon$ formula indicates.

So the $k-\varepsilon$ formula is in error with the data in the vicinity of the wall, overestimating the turbulent transport to/from the surface. Consequently, models of $k-\varepsilon$ type tend to overpredict skin friction values and heat transfer rates.

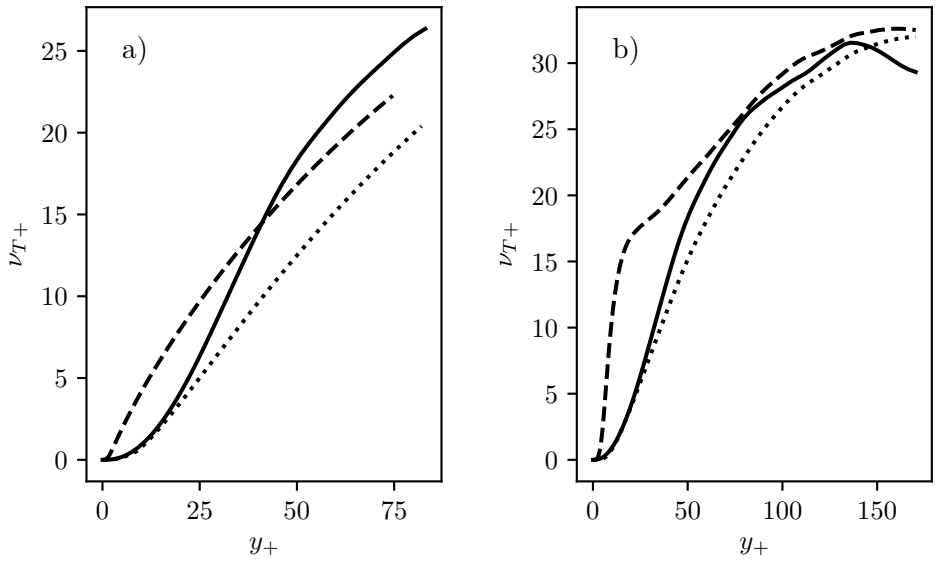

Figure 1.1: a) Predictions of eddy viscosity provided by models. - - - - $k-\varepsilon$ model; ····· $k-\varphi$ model (section 2.4); b) Prediction by formulas for eddy viscosity substituted with data from DNS of turbulent channel flow, $Re_\tau = 395$ [1]. - - - - $0.09k^2/\varepsilon$; ····· $0.22\overline{v^2}T$; Both figures: —— exact ν_T.

A quick solution lies in damping the viscosity according to the data by simply "fitting" the exact profile. A damping function of the Van Driest type has to be introduced in the eddy viscosity formula:

$$\nu_T = C_\mu f_\mu \frac{k^2}{\varepsilon}.$$

There is a bedazzling amount of proposed wall-damping functions, which is a testimony to their ineffectiveness. The use of a wall damping function not only introduces additional numerical stiffness, wall damping schemes fitted to zero pressure gradient (or channel flow) boundary layer data fail to correctly predict flows subjected to adverse pressure gradients.

Perhaps full second-moment closure modeling can be helpful in search of the more appropriate eddy viscosity formula. The transport equation for Reynolds stress contains a turbulent transport term, which can be closed again by gradient diffusion. Except for this time, eddy viscosity is a tensor (Daly & Harlow eddy viscosity formula [10]):

$$-\frac{\partial \overline{u_k u_i u_j}}{\partial x_k} = \frac{\partial}{\partial x_k}\left(C_\mu T \overline{u_k u_l} \frac{\partial \overline{u_i u_j}}{\partial x_l} \right).$$

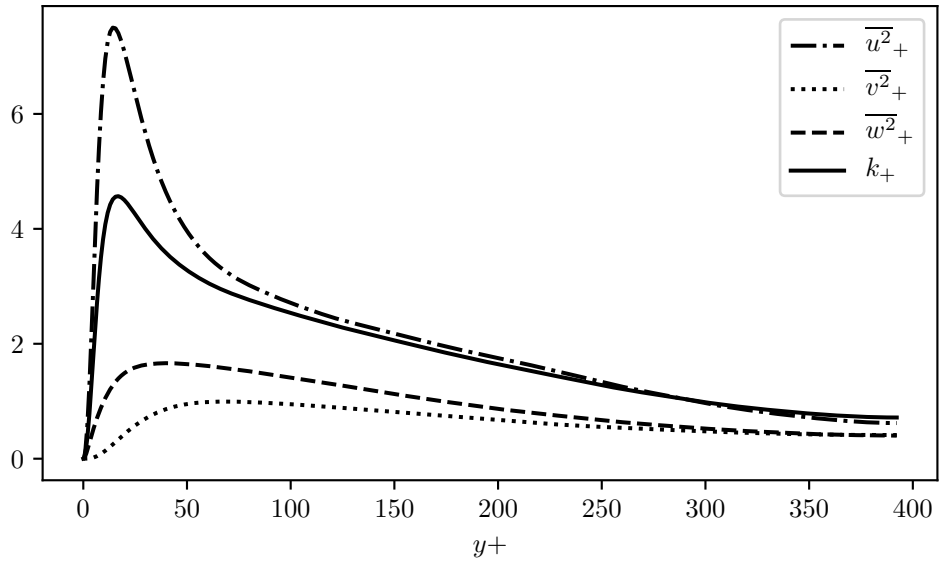

Figure 1.2: Reynolds stress profiles from DNS of turbulent channel flow for $Re_\tau = 395$ [1]. Kinetic energy profile is dominated by $\overline{u^2}$ component.

As the wall is approached, the dominant gradient is in the wall-normal direction, y. The turbulent transport model near a wall can be further approximated by only one term [8, p. 180]:

$$-\frac{\partial \overline{u_k u_i u_j}}{\partial y} = \frac{\partial}{\partial y}\left(C_\mu T \overline{v^2} \frac{\partial \overline{u_i u_j}}{\partial y}\right).$$

This suggests, using $\overline{v^2}$ as a velocity scale in the eddy viscosity formula rather than k. The value of constant C_μ is typically 0.22, very similar to those used in $\overline{v^2}$ – f models.

The failure of the $k-\varepsilon$ formula can be physically understood, by looking at the profiles of Reynolds stresses $\overline{u^2}, \overline{v^2}, \overline{w^2}$. The wall-normal one, $\overline{v^2}$ gets disproportionately suppressed compared to the tangential ones in the near-wall region, as one can see in figure 1.2. A glance back at the eddy viscosity profiles in turbulent channel flow reveals that the formula $C_\mu \overline{v^2} T$ is in very good agreement with the exact eddy viscosity profiles. The wall-normal Reynolds stress seems to be more closely related to turbulent transport than the tangential ones. Kinetic energy k is dominated by the bigger, tangential stress components and cannot predict the suppression of turbulent mixing in the vicinity of walls.

It seems a more appropriate energy scale for the eddy viscosity was found. The only thing missing is the equation that models the suppression of $\overline{v^2}$ near walls. Again, second-moment closure modeling has to be mentioned to properly introduce elliptic relaxation. At the same time, intricate mathematical

details will be omitted, for the sake of brevity. The following text will at least partially explain the structure of the source terms for the $\overline{v^2}$ equation encountered in the succeeding chapter. We shall discuss now the redistribution tensor $\wp_{ij}$ in the transport equation for the Reynolds stresses:

$$\wp_{ij} = -(\phi_{ij} + \varepsilon_{ij} - \frac{2}{3}\varepsilon\delta_{ij}).$$

For the sake of modeling, it contains several tensors lumped together. The crucial part is to correctly model the pressure contribution to the redistribution tensor ϕ_{ij}, which is defined by:

$$\phi_{ij} = \frac{1}{\rho}\left(\overline{u_i\frac{\partial p}{\partial x_j}} + \overline{u_j\frac{\partial p}{\partial x_i}}\right). \tag{1.8}$$

The redistribution tensor can be decomposed into "slow" $\wp_{ij}^{slow}$ and "rapid" $\wp_{ij}^{rapid}$ parts [8, Chap. 7]. This decomposition comes from the structure of the right-hand side of the equation (Poisson equation) for fluctuating pressure derived from incompressible Navier-Stokes equations.

The slow part can be modeled quite effectively with a simple Rotta model [11]:

$$\wp_{ij}^{slow} = -C_1\varepsilon a_{ij}, \tag{1.9}$$

where the tensor anisotropy a_{ij} is defined by:

$$a_{ij} = \frac{\overline{u_iu_j}}{k} - \tfrac{2}{3}\delta_{ij}.$$

The equation (1.9) shall be rescaled by k and written only for the second diagonal component so that the reader can gain a sense of familiarity when encountering the equations for the $\overline{v^2} - f$ model. The mentioned equation is of the form:

$$\frac{\wp_{22}^{slow}}{k} = -C_1\frac{1}{T}\left(\frac{\overline{v^2}}{k} - \frac{2}{3}\right). \tag{1.10}$$

A commonly used model for the rapid part $\wp_{ij}^{rapid}$, which linearly depends on the mean velocity gradient, is the IP model (isotropization of production, [12]):

$$\wp_{ij}^{rapid} = -\tfrac{3}{5}(\mathcal{P}_{ij} - \tfrac{1}{3}\delta_{ij}\mathcal{P}_{ii}). \tag{1.11}$$

This model (again, rescaled by k) was also adopted in the equation for $\overline{v^2}$ in $\overline{v^2} - f$ model.

Models derived under the homogeneous assumption can be used even when all the variables are functions of the position but do not vary rapidly. But one encounters similar problems as with the $k - \varepsilon$ formula for eddy viscosity. As the wall is approached, quasi-homogeneous models for the redistribution

tensor give erroneous predictions. Both the slow and rapid parts of the redistribution tensor are modeled as low-order algebraic expansions in powers of the anisotropy tensor, therefore the presence of solid boundaries in the Poisson equation for the fluctuating pressure has to be omitted to justify the procedure. Solid walls exert multiple effects on velocity fluctuations. The no-slip condition imposes the viscous dampening of the velocity fluctuations, which is active in the immediate vicinity of the walls and suppresses the velocity fluctuations equally in all directions. The wall-blocking effect stems from impermeability constraint and cannot be deduced from Reynolds stress tensor transport equations. It causes suppression of the wall-normal velocity fluctuations and makes the near-wall turbulence highly anisotropic and forces the turbulence to approach the two-component state at the edge of the viscous sublayer, hence $\overline{u^2}, \overline{w^2} = \mathcal{O}(y^2), \overline{v^2} = \mathcal{O}(y^4)$ [13].

Elliptic relaxation attempts to model the kinematic blocking of the wall by imposing the correct limiting behavior of the redistribution tensor in near-wall regions through boundary conditions imposed on $f_{ij} = \wp_{ij}/k$. The elliptic operator $L^2(\nabla^2 - 1)$ will continuously blend near-wall and far-from-the-wall forms (homogenous models) of the redistribution tensor, as the distance from the solid boundaries increases. The elliptic relaxation equation has the form:

$$L^2 \frac{\partial^2 f_{ij}}{\partial x_k \partial x_k} - f_{ij} = \frac{\wp_{ij}^{slow} + \wp_{ij}^{rapid} + \varepsilon a_{ij}}{k} \tag{1.12}$$

To gain an intuition behind the non-local and elliptic nature of the kinematic blocking, consider reading [8, Sec. 7.3]. More extensive mathematical background and derivation of elliptic relaxation equations are available in the article [14].

Chapter 2

Formulations of $\overline{v^2} - f$ model

Elliptic relaxation equations further add to the complexity of full second-moment closure models. To obtain a computationally tractable model, which retains a characterization of near-wall anisotropy, one shall scrap full second-moment closure and keep only the equation for $\overline{v^2}$ of Reynolds stress tensor. The model will still use equations for turbulence kinetic energy and dissipation rate as scale-determining equations, but the eddy viscosity formula is redefined:

$$\nu_T = C_\mu \overline{v^2} T. \tag{2.1}$$

Let the reader be reminded that $\overline{v^2}$ is not one of the diagonal components of the Reynolds stress tensor in this context, but a scalar quantity used to properly damp the eddy viscosity in the vicinity of the wall. In channel flows, with the usual choice of the cartesian set of coordinates, $\overline{v^2}$ corresponds to a wall-normal component. This component gets disproportionately suppressed compared to other diagonal components near the wall. Far away from the walls, the qualitative behavior of $\overline{v^2}$ should be the same as that of k. In such quasi-homogeneous conditions, a model of $\overline{v^2} - f$ type should be qualitatively equivalent to the $k - \varepsilon$ model. The additional transport equation for the $\overline{v^2}$ reads:

$$\frac{D\overline{v^2}}{Dt} = kf - \overline{v^2}\frac{\varepsilon}{k} + \frac{\partial}{\partial x_j}\left[\left(\nu + \frac{\nu_T}{\sigma_k}\right)\frac{\partial \overline{v^2}}{\partial x_j}\right]. \tag{2.2}$$

The same logic applies to the term kf, it's not a component of a redistribution tensor, but a scalar field, representing the redistribution of energy between the stream-wise components and a wall-normal one. The following elliptic equation has to be solved to obtain f:

$$L^2 \frac{\partial f}{\partial x_j \partial x_j} - f = \frac{1}{T}(C_1 - 1)\left[\frac{\overline{v^2}}{k} - \frac{2}{3}\right] - C_2 \frac{\mathcal{P}_k}{k}. \tag{2.3}$$

Turbulent length scale L is determined as:

$$L = C_L \max\left(\frac{k^{3/2}}{\varepsilon}, C_\eta \frac{\nu^{3/4}}{\varepsilon^{1/4}}\right). \tag{2.4}$$

A lower bound on the length scale is imposed for the same reasons as the one for the correlation time scale. A vanishing length scale at the walls would make equation (2.3) singular. Near-wall length scales collapse well to the Kolmogoroff length scale $\nu^{3/4}/\varepsilon^{1/4}$. Much to someone's surprise, $\overline{v^2} - f$ models are very sensitive to the value of C_η.

2.1 Durbin's original $\overline{v^2} - f$ model

The original version uses the equations (2.2, 2.3) in their exact form. The model coefficients are the following [8, Sec. 7.3]:

$$\begin{aligned}
&C_\mu = 0.19,\ \sigma_k = 1.0, \sigma_\varepsilon = 1.3 \\
&C_{\varepsilon_1} = 1.4\left[1 + 0.045\sqrt{\frac{k}{\overline{v^2}}}\right],\ C_{\varepsilon_2} = 1.9 \\
&C_1 = 1.4,\ C_2 = 0.3,\ C_L = 0.3,\ C_\eta = 70.
\end{aligned}$$

The formula for C_{ε_1} is just a simple blending function, as the wall is approached, the $\overline{v^2}$ variable gets suppressed, C_{ε_1} will have a higher value, therefore dissipation is enhanced near the wall.

Boundary conditions at no-slip boundaries for $k, \overline{v^2}$ are homogenous (Dirichlet). ε satisfies previously derived asymptotic relation (1.7). The boundary condition for f can also be derived by considering the near-wall balance of terms in the $\overline{v}^2$ equation:

$$0 = kf - \varepsilon\frac{\overline{v^2}}{k} + \nu\frac{\partial^2\overline{v^2}}{\partial y^2}.$$

We further have to assume that as $y \to 0$, $\overline{v^2} = \mathcal{O}(y^4)$. Thus the equation above can be rewritten to:

$$0 = kf - \varepsilon\frac{\overline{v^2}}{k} + 12\nu\frac{\overline{v^2}}{y^2}.$$

Substituting the asymptotic relation for k, the following asymptotic behaviour for f is derived:

$$f \to -5\varepsilon\frac{\overline{v^2}}{k^2} = -20\frac{\nu^2\overline{v^2}}{\varepsilon y^4} \qquad as \qquad y \to 0. \tag{2.5}$$

Such a boundary condition can lead to serious numerical problems when used with segregated solvers. The equation above suggests, that $f = \mathcal{O}(1)$ at

the boundary. However, at the start of the iteration procedure, the numerator and denominator can have very different orders. This causes this fraction to essentially "blow up" during a real computation. As the denominator varies with y to the fourth power, the model cannot be used on cases with highly refined mesh near the walls (typically with $y_+ < 1$ or even less). But to correctly capture the "wall-blocking" effects by elliptic relaxation, exactly a high near-wall resolution of the mesh should always be considered.

2.2 $\zeta - f$ model of Hanjalić

A quick inspection of (2.5) reveals that a substantial computational advantage could be gained from using streamline-normal anisotropy $\zeta := \overline{v^2}/k$ rather than $\overline{v^2}$. A transport equation can be derived just from transport equations for k and $\overline{v^2}$ by realizing that:

$$\frac{D\left(\frac{\overline{v^2}}{k}\right)}{Dt} = \frac{D\overline{v^2}}{Dt}\frac{1}{k} - \frac{Dk}{Dt}\frac{\overline{v^2}}{k^2}.$$

After substituting the right hand side of (1.2) and right hand side of (2.2) and considerable amount of algebra, the equation for ζ is obtained:

$$\frac{D\zeta}{Dt} = f - \zeta\frac{\mathcal{P}_k}{k} + \frac{\partial}{\partial x_j}\left[\left(\nu + \frac{\nu_T}{\sigma_k}\right)\frac{\partial\zeta}{\partial x_j}\right] + \frac{2}{k}\frac{\partial k}{\partial x_j}\frac{\partial\zeta}{\partial x_j}\left(\nu + \frac{\nu_T}{\sigma_k}\right). \tag{2.6}$$

Hanjalić [15] omits the cross-diffusion term and replaces the σ_k coefficient with σ_ζ with a different value. The right-hand side of the elliptic equation for f is a little bit different. Instead of using the IP model for redistribution tensor, a more advanced SSG model was adopted. The SSG model supposedly better captures the near-wall anisotropy in boundary layers. It is not clear to the author how even a slight improvement over the original model could be achieved when such a "drastic surgery" on the SSG model was performed. The equation reads:

$$L^2\frac{\partial f}{\partial x_j \partial x_j} - f = \frac{1}{T}\left(c_1 + C_2'\frac{\mathcal{P}_k}{\varepsilon}\right)\left(\zeta - \frac{2}{3}\right). \tag{2.7}$$

The constants of the model are the following:

$$C_\mu = 0.22,\ C_{\varepsilon 1} = 1.4\left(1.0 + \frac{0.012}{\zeta}\right),\ C_{\varepsilon 2} = 1.9$$
$$c_1 = 0.4,\ C_2' = 0.65, C_L = 0.36,\ C_\eta = 85$$
$$\sigma_k = 1.0,\ \sigma_\varepsilon = 1.3,\ \sigma_\zeta = 1.2.$$

Main objective of this model is to be a numerically robust version of the original $\overline{v^2} - f$ model.The numerator and denominator of the boundary condition for f shall be now proportional to y^2. That is readily seen from the

near-wall balance:

$$0 = f + \nu\frac{\partial^2\zeta}{\partial y^2};$$
$$f \to -\varepsilon\frac{\zeta}{k} = -\frac{2\nu\zeta}{y^2} \qquad as \qquad y \to 0.$$

This asymptotic behavior is equivalent to that of dissipation rate but with an opposite sign. The author's experience with implementing this model and using it with a segregated solver suggests that even this type of regularization wasn't enough. Values of $|f|$ near the solid boundaries weren't as high as in the case of the original model but were still too high for any of the attempted simulations to be convergent. f becomes a sink for the ζ variable near solid boundaries and can even force ζ to be negative. Not only are such values of anisotropy unrealizable, if ζ is negative, then consequently $\nu_T = C_\mu k\zeta T$ will be negative. Negative diffusion usually ends with the whole calculation diverging.

2.3 A version of $\overline{v^2} - f$ model by Lien and Durbin

To gain a numerically robust model, the boundary condition for f must be further simplified. Homogenous Dirichlet boundary condition can be obtained by change of the variable f:

$$f = \overline{f} - 5\varepsilon\frac{\overline{v^2}}{k^2}. \tag{2.8}$$

As can be seen from (2.5), $\overline{f}$ is indeed zero at the wall. The new set of equations are:

$$\frac{D\overline{v^2}}{Dt} = k\overline{f} - 6\varepsilon\frac{\overline{v^2}}{k} + \frac{\partial}{\partial x_j}\left[\left(\nu + \frac{\nu_T}{\sigma_k}\right)\frac{\partial\overline{v^2}}{\partial x_j}\right]; \tag{2.9}$$

$$L^2\frac{\partial^2\overline{f}}{\partial x_j\partial x_j} - \overline{f} = \frac{1}{T}(C_1 - 1)\left[\frac{\overline{v^2}}{k} - \frac{2}{3}\right] - C_2\frac{\mathcal{P}_k}{k} - 5\varepsilon\frac{\overline{v^2}}{k^2} + 5L^2\frac{\partial^2}{\partial x_j\partial x_j}\left(\varepsilon\frac{\overline{v^2}}{k^2}\right). \tag{2.10}$$

Following Lien and Durbin [16], the term $5L^2\nabla^2(\varepsilon\overline{v^2}/k^2)$ is neglected in the $\overline{f}$ equation. The constants of the model are:

$$C_\mu = 0.22,\ \sigma_k = 1.0,\ \sigma_\varepsilon = 1.3,$$
$$C_{\varepsilon_1} = 1.4\left[1 + 0.05\sqrt{\frac{k}{\overline{v^2}}}\right],\ C_{\varepsilon_2} = 1.9,$$
$$C_1 = 1.4,\ C_2 = 0.3,\ C_L = 0.23,\ C_\eta = 70.$$

Now the boundary value problem for f is well-posed, the equation for f is decoupled from $\overline{v^2}$ one and the model is much better suited for use with

segregated solvers. Initial calculations conducted with this model converged successfully, even without elaborate care for implementation. Although this version of the model is sufficiently "code friendly", the term neglected in the $\overline{f}$ equation can be important in boundary layer regions. Coming from the usual log-layer assumptions, this term doesn't vanish in the log-layer. If we assume that $L = \mathcal{O}(y),\ \varepsilon = \mathcal{O}(y^{-1}),\ k, \overline{v^2} = \mathcal{O}(1)$ in the log-layer, the neglected term is even of the same order as $-5\varepsilon\overline{v^2}/k^2$ in the $\overline{f}$ equation.

2.4 A robust $\varphi - f$ formulation

The objective of this formulation is to be "code friendly" as the previous one but also to be in some sense more "consistent" with the original $\overline{v^2} - f$ model. We start again by defining streamline-normal anisotropy $\varphi := \overline{v^2}/k$. The transport equation for this variable was already derived when the $\zeta - f$ model was introduced, see (2.6). A substitution for f is suggested, that will force the new variable $\overline{f}$ to vanish at solid boundaries:

$$f = \overline{f} - 2\frac{\nu}{k}\frac{\partial\varphi}{\partial x_j}\frac{\partial k}{\partial x_j} - \nu\frac{\partial^2\varphi}{\partial x_j\partial x_j}.$$

The new substitution removes all the viscous terms in the φ equation:

$$\frac{\mathrm{D}\varphi}{\mathrm{D}t} = f - \varphi\frac{\mathcal{P}_k}{k} + \frac{\partial}{\partial x_j}\left(\frac{\nu_T}{\sigma_k}\frac{\partial\varphi}{\partial x_j}\right) + \frac{2}{k}\frac{\partial k}{\partial x_j}\frac{\partial\varphi}{\partial x_j}\frac{\nu_T}{\sigma_k}. \tag{2.11}$$

The equation for $\overline{f}$ will be simplified in the same fashion as in the formulation of Durbin and Lien. The laplacian of terms involved in the change of variable f is neglected: $\nu L^2\nabla^2\left(2/k\nabla\varphi\nabla k + \nabla^2\varphi\right)$. As was shown in [17], this is a far less drastic simplification. One finally obtains an equation for $\overline{f}$:

$$L^2\frac{\partial^2\overline{f}}{\partial x_j\partial x_j} - \overline{f} = \frac{1}{T}(C_1 - 1)\left(\varphi - \frac{2}{3}\right) - C_2\frac{\mathcal{P}_k}{k} - 2\frac{\nu}{k}\frac{\partial\varphi}{\partial x_j}\frac{\partial k}{\partial x_j} - \nu\frac{\partial^2\varphi}{\partial x_j\partial x_j}. \tag{2.12}$$

For most of the applications of this work, the $\varphi - f$ formulation of the $\overline{v^2} - f$ model will be used. At last, the coefficients of the model are the following [17]:

$$\begin{aligned}
&C_\mu = 0.22,\ \sigma_k = 1.0,\ \sigma_\varepsilon = 1.3,\\
&C_{\varepsilon_1} = 1.4\left[1 + 0.05\sqrt{\frac{1}{\varphi}}\right],\ C_{\varepsilon_2} = 1.9,\\
&C_1 = 1.4,\ C_2 = 0.3,\ C_L = 0.25,\ C_\eta = 110.
\end{aligned}$$

2.5 Modifications of $\overline{v^2} - f$ model concerned with the behaviour outside the near-wall region

A little insight into the relationship between the $\overline{v^2} - f$ a $k - \varepsilon$ model in regions far away from solid boundaries shall be provided. A great starting

point is homogeneous, parallel shear flow. A well-known result regarding the equilibrium value of production to dissipation ratio applies:

$$\left(\frac{\mathcal{P}_k}{\varepsilon}\right)_\infty = \frac{C_{\varepsilon 2} - 1}{C_{\varepsilon 1} - 1} \tag{2.13}$$

Under the assumption of homogeneity, the equation for f (2.3) reduces to an algebraic equation:

$$-f_{hom} = \frac{1}{T}(C_1 - 1)\left(\frac{\overline{v^2}}{k} - \frac{2}{3}\right) - C_2\frac{\mathcal{P}_k}{k}. \tag{2.14}$$

Substituting (2.14) to homogeneous simplification of (2.2) yields the following evolution equation:

$$\frac{d}{dt}\left(\frac{\overline{v^2}}{k}\right) = \frac{\varepsilon}{k}\left[(C_1 - 1)\left(\frac{2}{3} - \frac{\overline{v^2}}{k}\right) + \left(C_2 - \frac{\overline{v^2}}{k}\right)\frac{\mathcal{P}_k}{\varepsilon}\right]. \tag{2.15}$$

Equilibrium value $(\overline{v^2}/k)_\infty = 0.3683$ can be obtained from (2.15) by equaling the right-hand side to zero and substituting production to dissipation ratio with its equilibrium formula from (2.13). In these specific conditions, eddy viscosity obtained from $\overline{v^2} - f$ model doesn't stray too far from the $k - \varepsilon$ one:

$$\nu_T = C_\mu \frac{k^2}{\varepsilon}\left(\frac{\overline{v^2}}{k}\right)_\infty \doteq 0.081\frac{k^2}{\varepsilon}$$

It turns out that in regions far away from the wall, such conditions are seldom satisfied. The ratio $(\overline{v^2}/k)$ or φ can certainly be bigger than its equilibrium value. All values of φ bounded from below by 0 and from above by 2 are realizable. Thus eddy viscosity predicted by the $\overline{v^2} - f$ model can be several times higher than the one predicted by the standard $k - \varepsilon$ model. In [18], the authors were perhaps too concerned with this fact. According to their line of reasoning, the wall-normal anisotropy should never be bigger than the isotropic value of 2/3. Hence a limiter on the source term in $\overline{v^2}$ equation was designed:

$$\overline{v^2}_{source} = \min\{kf, kf_{hom}\}. \tag{2.16}$$

We can go further and enforce a limiter on eddy viscosity:

$$\nu_T = \min\left\{0.09\frac{k^2}{\varepsilon}, C_\mu\overline{v^2}T\right\}. \tag{2.17}$$

These two modifications don't seem reasonable enough to implement. The value 0.09 comes from measurements of shear stress intensity ratio $\overline{uv}/k \approx 0.3$ done in the boundary layer regions. Actual values of this ratio further from the wall are not available. One should not cling too much to being consistent

with the value of $C_\mu = 0.09$, its domain of validity is constrained to boundary layers.

A more relevant question needs to be asked: Can eddy viscosity determined by a $\overline{v^2}-f$ model be spuriously amplified? To illustrate how such amplifications can occur, we shall inspect the following equation for f simplified under log-layer assumptions:

$$L^2 \frac{\mathrm{d}^2 f}{\mathrm{d}y^2} - f = f_{hom} \tag{2.18}$$

Now bearing in mind the definition of f_{hom} in (2.14), it turns out $f_{hom} = \mathcal{O}(1/y)$ in the log-layer. This result is immediately seen from the fact that both terms contained in f_{hom} are proportional to $\sqrt{C_\mu} u_\tau / \kappa y$. Since the log-layer length scale is linear in y, one can see that, the solution to equation (2.18) is $f = \Gamma f_{hom}$, where Γ is some amplification factor. Here comes the problem: $\Gamma \neq 1$ and especially $\Gamma > 1$ in the log layer. This means that the "homogeneous" model of redistribution tensor can get amplified by the elliptic relaxation operator, which is a source term in the equation for $\overline{v^2}$. This consequently leads to spurious amplification of eddy viscosity. One can tackle this problem in two ways: rescaling the redistribution tensor by $k\varepsilon$ (then $f_{hom} = \mathcal{O}(1)$ since $\varepsilon = \mathcal{O}(1/y)$) or modify the elliptic relaxation operator in some way. Although the author deemed this issue worth exploring, none of the modifications mentioned in [19] were implemented.

Chapter 3

Case of an impinging jet

The axisymmetric jet impinging normally on a flat plate is a case (designated as case025) in the classic collection database of ERCOFTAC [3]. The practical application of an impinging jet is cooling since such flow configuration can very effectively enhance heat transfer rates. The chapter's main objective consists of predicting local Nusselt number distribution as a function of radial distance from the jet centerline.

3.1 Note on the experimental data

Several different experimental measurements of the heat transfer rates were conducted [4, 2, 5, 20]. As can be seen from the figure 3.1, Nusselt number distribution depends qualitatively on nozzle-to-plate spacing H/D. For cases $H/D \geq 4$, Nusselt numbers decrease monotonically with the radial distance from the jet centerline. For the cases, $H/D < 4$, the heat transfer characteristics are more complicated. The data in figure 3.1 indicate a secondary maximum in Nusselt numbers occurring in the range $1 \leq r/D \leq 2$. More recent data [5] for nozzle-to-plate spacing $H/D = 2$ plotted in figure 3.2 even show the existence of the primary peak, occurring approximately at the edge of the nozzle. As was suggested in the article [5], turbulent intensity peaks close to the inner circumference of the nozzles. This corresponds to large-scale toroidal vortices striking the plate, which for low nozzle-to-plate spacings didn't have enough time to completely diffuse. The secondary peak can be attributed to the transition from the laminar to the turbulent boundary layer in the spreading wall jet region $r/D \geq 2$. The distribution of Nusselt numbers for $H/D = 6$ doesn't have these characteristics. Authors of the article [20] also measured turbulence intensity measured along the centerline of the jet. It shows a gradual increase with going downstream and peaks at $H/D \approx 7$. The centerline turbulence intensity for the case $H/D = 6$ is approximately 4 times larger than for the $H/D = 2$ case, so the boundary layer stays fully turbulent even in the

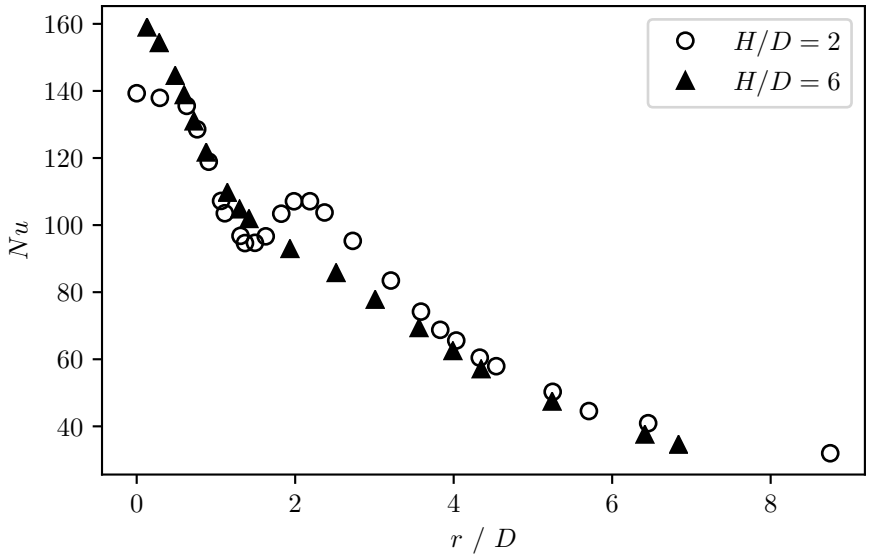

Figure 3.1: Nusselt number distributions for two different nozzle-to-plate spacings, $Re = 23\,750$. Data obtained from Baughn et. al (1989) [2].

stagnation region. In the case $H/D = 2$, the boundary layer is laminar until the stabilizing pressure gradient vanishes.

There seems to be a discrepancy among the experimental data for the $H/D = 2$ case, as figure 3.2 shows various measurements for similar Reynolds numbers (Reynolds number is based on the bulk velocity and the diameter of the nozzle). Eventually, the author chose to validate subsequent predictions with the data measured for $Re = 2.375 \times 10^4$, because they are closest to the data with the highest spatial resolution ($Re = 2.5 \times 10^4$).

3.2 Computational setup

3.2.1 Numerical method

The equations were discretized with the finite volume method and computations were done with various solvers implemented in OpenFoam, an open-source finite volume library. See [21], for a comprehensive introduction. The convective terms were discretized with the second-order upwind scheme [21, Sec. 11.5.2]. The Navier-Stokes equations were solved by an iterative Picard-like segregated algorithm called SIMPLE (Semi Implicit Method for Pressure Linked Equations)[21, Chap. 15].

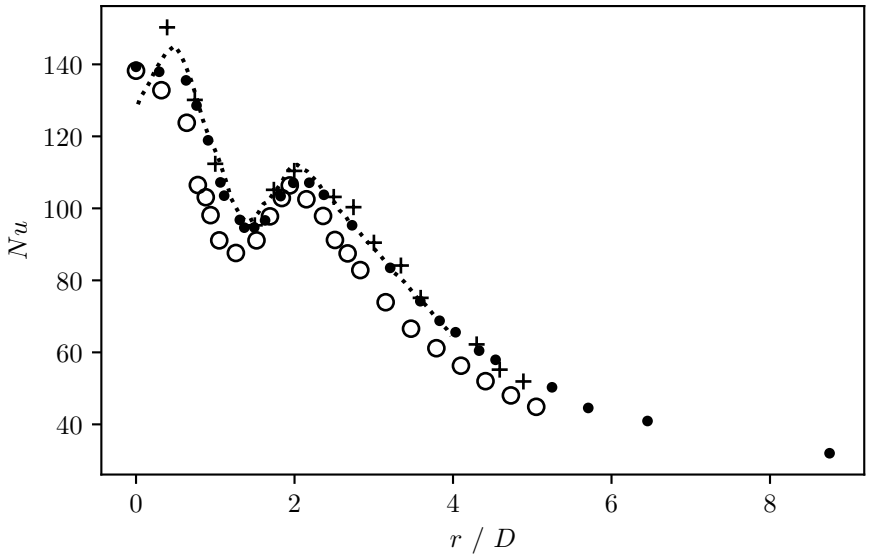

Figure 3.2: Experimentally obtained Nusselt number distributions for the impinging jet with nozzle-to-plate spacing H/D = 2. ○ Baughn et. al (1992), Re = 23000 [3]; • Baughn et. al (1989), Re = 23750 [2]; + Baughn et. al (1991), Re = 23300 [4]; ····· Lee & Lee (1999), Re = 25000 [5]

3.2.2 Mesh and boundary conditions

At first, a fully two-dimensional mesh was considered. Then it was replaced by a wedge-shaped mesh. This geometry of the domain is more appropriate because the impinging jet flows on circular plates are axisymmetric and not two-dimensional. Although the subsequent computations were all three-dimensional, the dominant velocity components were in the normal and radial direction from the jet centerline, the tangential one was negligible. It was apparent that the two-dimensional approximation was justified, but still, the Nusselt number distributions obtained from the wedge-shaped mesh were in better agreement with the experimental data.

The length of the nozzle was set only to approximately two diameters of the nozzle (which had one inch in diameter, so the diameter D was set precisely to D = 26.5 mm), and converged turbulence quantities were set at the nozzle inlet. This choice is in contrast with the article [22], where a rather large nozzle length $L_{nozzle} = 72D$ was employed so that the solution would be insensitive to the prescribed turbulence intensity at the inlet. It was found from the author's own experience with $k - \varepsilon$ models that prescribing "flat" profiles of turbulence quantities as inlet boundary conditions can frequently lead to the iterative procedure diverging. A large nozzle length also implies additional computational overhead, which is strictly unnecessary. The shape of the domain can be observed in figure 3.3, the distance of the "horizontal

outlet" from the plate was exactly two nozzle diameters. This particular configuration of the domain was met with difficulties regarding the stability of the iterative procedure. A massive reentering of the fluid through the horizontal outlet was encountered in the early stages of the computation, sometimes leading to divergence. In [23], the authors suggest that the top outlet boundary should be at least as high as the location of the nozzle inlet to prevent such problems. However, these complications can be dealt with more straightforwardly, without modifying the shape of the domain. At the early stage of the iterative procedure, the solution variables were aggressively under-relaxed until a semi-converged solution was obtained, in which almost none of the reentering of the fluid was present. Then the computation was restarted, with less drastic under-relaxation.

At the nozzle inlet Dirichlet boundary conditions were set for mean velocity and other turbulence quantities, which were obtained from separate one-dimensional channel flow computation, where a target bulk velocity U_b can be set. The Reynolds number based on the bulk velocity, $Re = U_b D/\nu$ was set to 2.3×10^4 in accordance with the ERCOFTAC case. The value of kinematic viscosity was set to $\nu = 1.552 \times 10^{-5}\,\mathrm{m^2 s^{-1}}$, therefore the value of bulk velocity was $U_b \doteq 13.47\,\mathrm{ms^{-1}}$.

Before describing the treatment of the outlet boundaries and pressure boundary conditions, two simple functions have to be introduced, to avoid any confusion. First one is $pos0(x)$:

$$pos0(x) = \begin{cases} 1, & \text{if } x \geq 0 \\ 0, & \text{otherwise} \end{cases},$$

the second one is $neg(x)$:

$$neg(x) = \begin{cases} 1, & \text{if } x < 0 \\ 0, & \text{otherwise} \end{cases}.$$

Pressure boundary conditions are closely related to the SIMPLE algorithm. At the inlet boundary a special non-homogenous Neumann boundary condition (called "fixedFluxPressure") was prescribed, according to the formula:

$$\frac{\partial p}{\partial \mathbf{n}_f} = \left(\frac{1}{a_f} H(\mathbf{U})_f - \mathbf{U}_f \cdot \mathbf{S}_f \right) \frac{a_f}{S_f}.$$

Bold fonts denote vectors and subscript f signifies quantities interpolated to the face centers of cells. S_f denotes the area of a particular face of the cell and $\mathbf{S}_f = S_f \mathbf{n}_f$, where $\mathbf{n}_f$ is an outward normal of the face. Operator H is a shorthand notation used in OpenFOAM to denote an affine operator resulting from the reinterpretation of the discretized momentum equation written for any cell center of the mesh (subscript c means cell center):

$$\mathbf{U}_c = \frac{1}{a_c} H(\mathbf{U}) - \frac{1}{a_c} \nabla P_c.$$

Consequently, any additional sources and terms coming from the implicit under-relaxation of the equation are absorbed in this operator. At last, a denotes the diagonal coefficient of the matrix assembled from the finite volume discretization of the momentum equation. This boundary condition ensures that the pressure gradient at the boundary is consistent with the momentum predictor equation and enhances the convergence rate of the SIMPLE algorithm.

At the outlet boundaries total pressure $P_0 = 0$ as a Dirichlet boundary condition was specified. In OpenFOAM, the "totalPressure" boundary condition relates the static pressure P (solution variable) to the total one in the following way:

$$P = P_0 - \tfrac{1}{2}(1 - pos0(\phi))|\mathbf{U}_c^2|,$$

where ϕ is the momentum flux and $\mathbf{U}_c$ is the velocity at the center of cells adjacent to the boundary. We can see, in the case of outflow $\phi > 0$, static pressure is equal to the total pressure.

For turbulence quantities such as kinetic energy k or dissipation rate ε a special type of Robin boundary conditions were prescribed at the outlet boundaries. In OpenFOAM, such conditions are called mixed and the boundary value x_b of a general field x is imposed according to the formula:

$$x_b = wx_D + (1 - w)\left(x_c + \frac{1}{\delta_c}\frac{\partial x}{\partial \mathbf{n}_f}\right), \tag{3.1}$$

where δ_c is the distance of the boundary face center to the corresponding center of the cell. Dirichlet boundary condition x_D, Neumann boundary condition $\partial x/\partial \mathbf{n}_f$ and weighting function w are left to specify. In particular, the "inletOultet" boundary conditions were used, where $\partial x/\partial \mathbf{n}_f = 0$ and the Dirichlet boundary condition x_D (called "inletValue") is left to be set by the user. The weighting function is specified as:

$$w = 1 - pos0(\phi).$$

In case of outflow $\phi > 0$, equation (3.1) reduces to $x_b = x_c$ and that coincides with the homogenous Neumann boundary condition in the context of finite volume discretization. For the inflow case, $\phi < 0$, the boundary value is set to the one prescribed by the user. For kinetic energy and dissipation rate very small "inlet" values were used, so that the stability issues related to the massive reentering of the fluid through outlet boundaries at the early stages of the iteration process were not further exacerbated. The only exception is φ, for which the isotropic value of 2/3 was specified.

Analogous outlet boundary conditions to the "inletOulet" were used for the mean velocity, in OpenFOAM called "pressureInletOutletVelocity". The velocity components at the boundary faces U_{bi} are set in the following way:

$$U_{bi} = (\delta_{ij} - w_{ij})U_{cj}. \tag{3.2}$$

The weighting function is now a symmetric tensor defined as:

$$w_{ij} = neg(\phi)(\delta_{ij} - n_{fi}n_{fj}).$$

Again we can see that in the outflow case, $\phi > 0$, the formula (3.2) sets the homogenous Neumann boundary condition for the velocity components. In the case of the inflow, $\phi < 0$ the formula (3.2) sets only the normal components extracted from $\mathbf{U}_c$ as the boundary value.

Treatment of no-slip boundaries, the plate, and the pipe wall was straightforward. Homogenous Dirichlet boundary conditions were employed for $\mathbf{U}$, k, f and φ. Boundary values for ε were obtained from the limiting expression (1.7) evaluated at the centers of cells adjacent to the no-slip boundaries. Computations were also done with some $k-\omega$ models, the corresponding limiting expression for ω at a no-slip boundary reads:

$$\omega \to \frac{6\nu}{\beta y^2} \quad as \quad y \to 0, \tag{3.3}$$

where β is a constant, multiplying the sink term $-\beta\omega^2$ in the ω equation, the precise form of the equation will be discussed in section 4.3.

A grid refinement study was done and the results are available in the appendix A.1.

3.2.3 An advection-diffusion equation for temperature

Since we are primarily interested in predicting heat transfer rates to/from the plate, the following auxiliary equation for thermodynamic temperature Θ (more precisely mean thermodynamic temperature) has to be solved:

$$\frac{\mathrm{D}\Theta}{\mathrm{D}t} = \frac{\partial}{\partial x_j}\left[\left(\frac{\nu}{Pr} + \frac{\nu_T}{Pr_T}\right)\frac{\partial\Theta}{\partial x_j}\right], \tag{3.4}$$

where the velocity-temperature correlation $\overline{u_j\theta}$ is modeled by additional "turbulent" thermal conductivity, which is analogous to the Boussinesq hypothesis for Reynolds stresses:

$$-\overline{u_j\Theta} = \frac{\nu_T}{Pr_T}\frac{\partial\Theta}{\partial x_j}. \tag{3.5}$$

The Prandl numbers were assumed to be constant, with $Pr = 0.7$ and $Pr_T = 0.85$. The inlet was treated as a Dirichlet boundary condition with a constant value of $\Theta_a = 293.16\ K$. The pipe wall boundary was assumed adiabatic, which means a homogenous Neumann boundary condition was employed. Both outlet boundaries were treated with the "inletOutlet" boundary condition described in the previous subsection, with the inlet value set to Θ_a. A Dirichlet boundary condition with a constant value $\Theta_w = \Theta_a + \Delta\Theta$, $\Delta\Theta = 15\ K$ was prescribed at the plate so that a near-wall temperature profile can

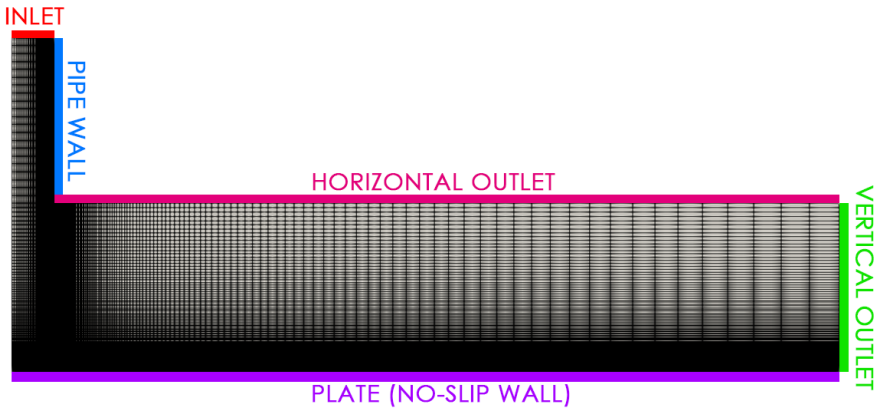

Figure 3.3: Computational domain with boundary conditions and mesh for the impinging jet.

develop. Consequently, the Nusselt numbers were defined as a normalized temperature flux from the plate:

$$Nu = \frac{D}{\Delta\Theta}\frac{\partial\Theta}{\partial y}\bigg|_w$$

Computation of the temperature field was always done as a post-processing step after computing the mean velocity field and eddy viscosity.

3.3 Early results

First, a more interesting case of nozzle-to-plate spacing $H/D = 2$ will be tackled. The $\varphi - f$ formulation of the $\overline{v^2} - f$ model was applied to obtain a prediction of the Nusselt number distribution displayed in figure 3.5. The figure reveals a gross overprediction of heat transfer rates in the region $0 \leq r/D \leq 3$. The prediction of the $\varphi - f$ model is contrasted with the prediction obtained by Wilcox's $k-\omega$ model (version from 2006, [24, Sec. 4.3]). The $k-\omega$ only slightly overpredicts the Nusselt numbers in the stagnation region but fails at predicting the supposed laminar-to-turbulent transition in the region $1 < r/D < 2$, also the wall-jet region $r/D > 2$ is underpredicted. In the region far away from the jet centerline $r/D \geq 3$ the $\varphi - f$ model is in good agreement with the experimental data.

Figure 3.4 can explain the failure of the $\varphi - f$ model, which suffers from spurious overproduction of turbulence kinetic energy in the stagnation region,

as the figure shows. The fact that the $\varphi - f$ model is a drastic simplification of the full Reynolds stress model now comes into play. Since it can be also interpreted as a $k - \varepsilon$ model augmented with an additional velocity scale intended to properly dampen the eddy viscosity in the near-wall regions. This indicates that as a linear eddy viscosity model, the $\varphi - f$ model will also inherit all the deficiencies of the Boussinesq hypothesis. As was stated at the end of the introduction, the production rate of turbulence kinetic energy is now quadratic in symmetric velocity gradient magnitude $\mathcal{P}_k \propto S_{ij}S_{ij}$.

Essentially two problems are encountered with such proportionality when it is compared with the formula for production rate defined in the context of a full Reynolds stress model $\mathcal{P}_k = 1/2\mathcal{P}_{ii}$. Not only is the latter one linear in the velocity gradient, but it's also just a trace of the production tensor - the diagonal components can have opposing signs and can partially cancel out. The expression $S_{ij}S_{ij}$ is a double contraction, the terms in the sum consist of a squared component of the symmetric velocity gradient. Firstly, this leads to an incorrect representation of the normal stress anisotropy (the formula $2\nu_T|S|^2$ predicts incorrect normal stress difference in pure straining flow [8, Sec. 6.4], [25]). Secondly, in cases exhibiting large strain rates, such as flows with stagnation regions, the formula $2\nu_T|S|^2$ overestimates the level of production rates, thus linear eddy viscosity models suffer from "stagnation point anomalies". The spurious overprediction of kinetic energy levels is however not an anomaly but a consequence of the Boussinesq hypothesis.

3.4 Ad hoc modifications dealing with stagnation anomaly

The following subsections will introduce and assess the performance of various limiters and modifications designed to suppress stagnation point anomalies.

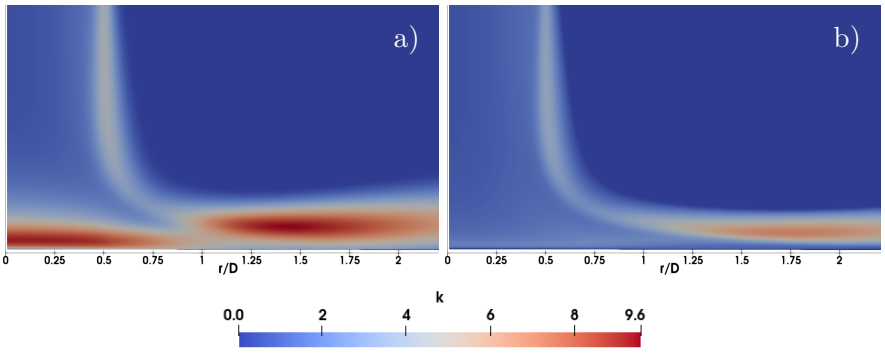

Figure 3.4: a) Kinetic energy field computed by $\varphi - f$ model. b) Kinetic energy field computed by $k - \omega$ model.

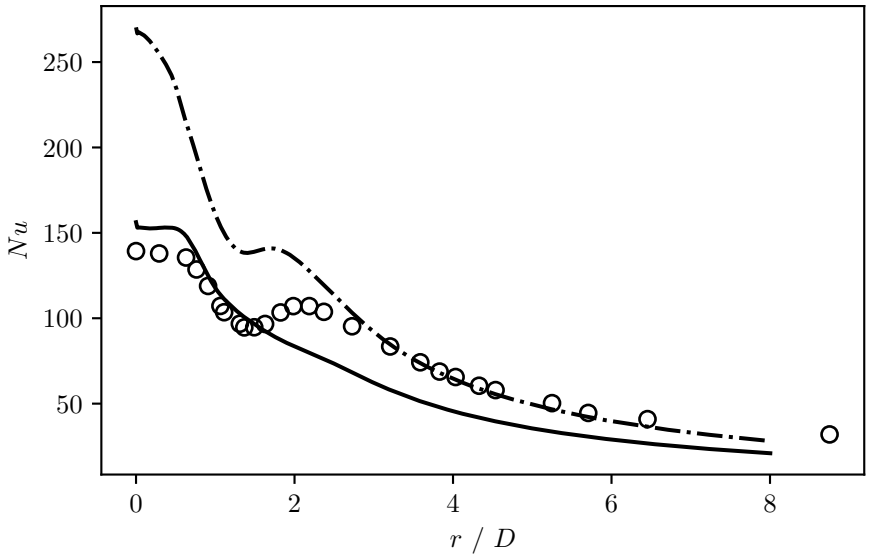

Figure 3.5: Nusselt number distribution computed by two different models. —— Wilcox's 2006 $k-\omega$ model; –·–·– $k-\varphi$ model; ○ Baughn et. al (1989), $Re = 23\,750$.

3.4.1 A realizability constraint

The symmetry of the Reynolds stress tensor is a convenient feature. Subsequently, the symmetric mean velocity gradient appears in the eddy viscosity formula:

$$\overline{u_i u_j} \;=\; 2\nu_T S_{ij} + \tfrac{2}{3} k \delta_{ij}, \tag{3.6}$$

and it can be exploited. A "realizability" constraint can be imposed upon the normal Reynolds stresses:

$$\forall \alpha : 0 \;\leq\; \overline{u_\alpha^2} \;\leq\; 2k, \tag{3.7}$$

and systematically derived. Since S_{ij} is a symmetric tensor, a unique coordinate system exists, in which the tensor is diagonal (principal axes) and the diagonal components λ_α are its eigenvalues. In such a coordinate system, the following statements hold:

$$\lambda_1^2 + \lambda_2^2 + \lambda_3^2 \;=\; |S|^2; \quad \lambda_1 + \lambda_2 + \lambda_3 \;=\; 0. \tag{3.8}$$

The second statement is an incompressibility condition $S_{ii} = 0$. Normal stresses can be written in the principal coordinate system:

$$\overline{u_\alpha^2} \;=\; -2\nu_T \lambda_\alpha + \tfrac{2}{3} k. \tag{3.9}$$

Durbin [26] derived a time-scale bound as a realizability constraint starting from the normal stress representation (3.9) using the equalities (3.8). In the case of $\varphi - f$ model, the expression reads:

$$T \leq \frac{C_{lim}}{3\varphi C_\mu} \frac{1}{\max \lambda_\alpha}, \tag{3.10}$$

where $\max \lambda_\alpha$ equals $\sqrt{|S|^2/2}$ in two dimensions, $\sqrt{2|S|^2/3}$ in three dimensions. Notice that the bound was constructed from fictitious pure strain in principal axes, irrespective of the actual structure of the symmetric gradient. Therefore the limiter can be active even when no stagnation regions are present. The reader shall keep this in mind.

We can see that the realizability constraint can be applied to any linear eddy viscosity model, the limiting formula will be slightly different based on the scales used to form eddy viscosity. The limiting formula (3.10) applied to $2\nu_T|S|^2$ a linearized bound on production rate of kinetic energy:

$$\mathcal{P}_k \leq \frac{C_{lim}}{\sqrt{3}} k|S|. \tag{3.11}$$

Similarly one can obtain an upper bound on the eddy viscosity:

$$\nu_T \leq \frac{C_{lim} k}{\sqrt{6}|S|}. \tag{3.12}$$

It's a common drawback of almost any ad hoc modification of turbulence models that one cannot fix the multiplicative constants in a standardized way. Unfortunately, such is also the case of the C_{lim} constant. A "recommended" value of 0.6 exists, but one cannot be certain that it is always the appropriate value. The value of C_{lim} is doomed to be a dangling degree of freedom, which can sometimes be finely tuned so that the model at hand can fit the data better.

The equation (3.11) in addition to bounding the Reynolds stress tensor can be applied as a stress limiter (limit only Reynolds stress), the equation (3.12) as a viscosity limiter (limit every instance of ν_T). The performance of all three limiters can be assessed by looking at figure 3.6. The time-scale limiter seems to provide the best results. The bounded time scale suppresses the eddy viscosity and the source terms in the ε equation are divided by the time scale, which results in enhanced dissipation rates in the regions where the time-scale bound is active. This mechanism is not present in the other two limiters, hence why they are less effective. In the case of the viscosity limiter, the dissipation rate enhancement is the only difference between the time-scale limiter, the supposed laminar-to-turbulent transition is predicted correctly, albeit the rise in heat transfer rates in the onset turbulent boundary layer is overpredicted. It's also important to note that the stress and viscosity limiters provide very similar results.

The time-scale limiter is surprisingly tricky to implement. But not in the sense of actual programming. The author was at first unsure where actually to apply it. When the time-scale limiter is applied, the production and viscosity

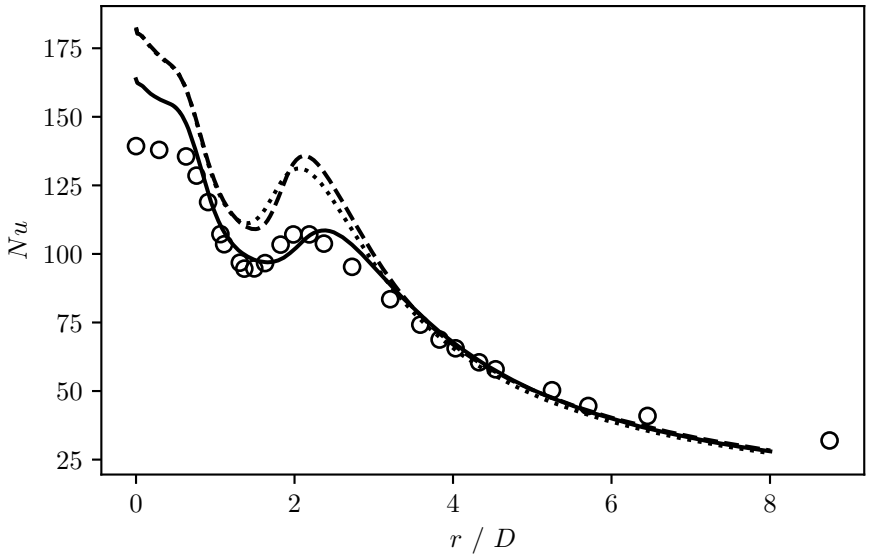

Figure 3.6: Nusselt number distributions obtained by applying different versions of realizability constraints on φ–f model. C_{lim} = 0.5 for all three limiters. ····· stress limiter (3.11); - - - - viscosity limiter (3.12); —— time-scale limiter (3.10); ○ Baughn et. al (1989), Re = 23750.

limiters are applied implicitly. The source and sink of the dissipation rate equation are divided by a time scale, so by limiting it, the dissipation rate can be further increased. All of this seems reasonable, but problems arise when the limiter is applied on time scales appearing in the equations for f or φ ($\overline{v^2}$). This is critical for the regularized Lien & Durbin version of the $\overline{v^2}$ – f model. The right hand side of (2.9) contains a sink $-6\varepsilon\overline{v^2}/k$, which comes from the substitution and should be reinterpreted as $-6\overline{v^2}/T$. This dimensionally consistent interpretation should be only done for the sake of the term being regular even when the wall is approached. The right-hand side of the equation (2.10), also contains terms divided by the time scale, again strictly for numerical reasons. For instance, the first term is divided by the time scale, but that is the Rotta model of the slow part of the redistribution tensor component rescaled by kinetic energy, as was demonstrated in (1.10). Applying the limiter in additional two equations of any formulation of the $\overline{v^2}$–f model can lead to divergence. Various terms in the f equation are divided by T, so f will get amplified. f is a source in φ ($\overline{v^2}$) equation, which then gets amplified. As φ ($\overline{v^2}$) is in the numerator of the bounding formula (3.10), it will further decrease the bounded time scale. Essentially a positive feedback loop develops, ending in the computation diverging. Authors of the article [27] reported the same problems. Converged solutions can be obtained by actually not applying the time-scale limiter in the f equation and by limiting

only the eddy viscosity in the φ ($\overline{v^2}$) equation. Incorporating the time-scale limiter into the $\varphi - f$ model was, to put it lightly, frustrating.

3.4.2 Kato - Launder modification

The culprit of the problem lies in the excessive production of turbulence kinetic energy in irrotational strain, then perhaps replacing $2\nu_T|S|^2$ to $2\nu_T|S||\Omega|$ can alleviate the issue. This is known as the Kato-Launder modification, first used for transient simulations around square cylinders [25]. The $k-\varepsilon$ model overproduced turbulence kinetic energy in stagnation regions and around sharp corners - small regions with strong acceleration and deceleration.

Three difficulties arise regarding this approach. Firstly, the Launder-Kato modification of the production rate predicts zero production of kinetic energy in irrotational strain, which is incorrect. Secondly, this modification of the production rate is not consistent with the conservation equation for mean kinetic energy $\frac{1}{2}|U|^2$, where a sink appears in the form $-\mathcal{P}_k$ (this is the rate at which kinetic energy of the mean flow is transferred to the kinetic energy of the fluctuations), except that it can only be derived as $-2\nu_T|S|^2$ [8, Sec. 6.4]. The most obvious difficulty is that this modification can spuriously produce kinetic energy in rotating frames of reference. Coordinate system independence requires that when dealing with rotating frames, one has to interpret $|\Omega|$ as the magnitude of the absolute vorticity in the inertial frame $|\Omega^A|$, where $\Omega^A_{ij} = \Omega_{ij} + \varepsilon_{ijk}\Omega^F_k$ and Ω^F is the rate of frame rotation. Thus in a pure straining flow in a rotating frame, the production rate $2\nu_T|S||\Omega^F|$ is proportional to the rate of frame rotation [8, Sec. 6.4]. In reality, frame rotation doesn't cause this effect. More often than not, frame rotation can have a strong stabilizing effect, sometimes even triggering the relaminarization of the flow.

Figure 3.8 showing the Nusselt number distribution indicates that the Kato-Launder modification is effective, albeit far less than the time-scale limiter. Figure 3.7 demonstrates that the region exhibiting large strain rates extends far above the boundary layer, where the fluid decelerates mainly in the direction of the streamlines. Thus the magnitude of the strain rate $|S|$ is much larger than the magnitude of vorticity $|\Omega|$ in this region. Consequently, the formula $2\nu_T|S||\Omega|$ will suppress the production rate, and the region of excessive kinetic energy observed in the left figure 3.4 is no longer present. Further inspection of the bottom of the figure 3.7 reveals that magnitudes of vorticity and strain rate are approximately equal in the boundary layer, hence the formula $2\nu_T|S||\Omega| \approx 2\nu_T|S|^2$ in close proximity of the plate. This fact can explain the overprediction of Nusselt numbers when compared with the time-scale limiter, which is active even in the boundary layer. At least the Kato-Launder modification preserves the secondary peak in the Nusselt numbers.

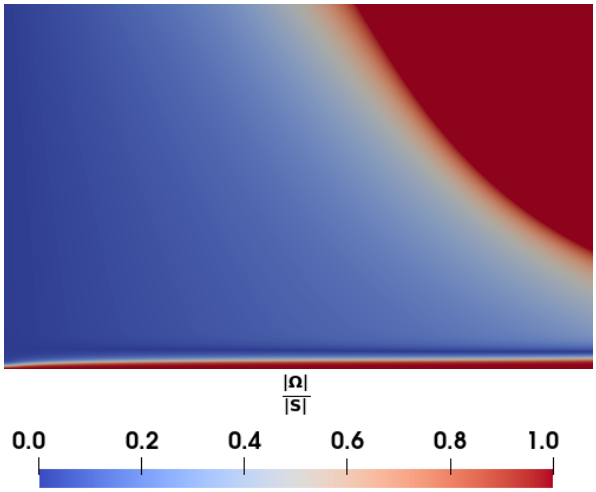

Figure 3.7: Ratio of vorticity and strain magnitudes in the region $0 \leq r/D \leq 0.5$ of the plate. The colormap was rescaled to emphasize that the ratio $|\Omega|/|S| \approx 1$ in the boundary layer.

3.4.3 Yap correction

Yap correction term was first introduced in Yap's doctoral thesis [28]. The motivation behind the term comes from the fact that for flows far from equilibrium (for instance flows where large velocity gradients or pressure gradients are present), the ε equation is not properly balanced, therefore the turbulence length scale $l = k^{1.5}/\varepsilon$ is much larger than the equilibrium length scale l_e. The equilibrium length scale comes from the log-layer scaling and is derived within the framework of the $k-\varepsilon$ model:

$$l_e \;=\; C_\mu^{-0.75}\kappa y.$$

The reader shall be notified that this expression doesn't denote a unique equilibrium length scale, since for the $k-\omega$ model the corresponding formula is $C_\mu^{0.25}\kappa y$. The additional source term in the ε equation derived from this conjecture is presented as the following:

$$S_\varepsilon \;=\; \max\left[0.83\left(\frac{l}{l_e}-1\right)\left(\frac{l}{l_e}\right)^2\frac{\varepsilon}{T}\;,\;0\right].$$

The Yap correction term has an interesting composition. The fraction ε/T is dimensionally consistent with the ε equation, while everything else is dimensionless. The ratio $(l/l_e)^2$ penalizes the excessive values of the turbulence length scale determined by the $k-\varepsilon$ model in terms of the equilibrium length scale. This ratio is a vehicle to drive the turbulence length scale to the equilibrium one. The expression (l/l_e-1) restricts the whole term to the near wall

regions, since the turbulence length scales are concave, they rise abruptly in the vicinity of the walls and outside the boundary layers vary steadily. The restriction is imposed by bounding the whole expression from below by zero.

When a strict validation approach is assumed to assess the performance of the Yap correction, the effectiveness of this modification cannot be denied - as can be seen in the figure 3.8, the needed reduction of the heat transfer rates is present. Other researchers also reported improved predictions of heat transfer rates for impinging flows [29, 30, 31]. But the figure 3.9 reveals that the whole conjecture about driving the turbulence length scale to equilibrium is at odds with the actual reality. Yap correction term clearly drives the computed length scale to the log-layer one (the location $r/D = 0.5$ was chosen, as it is in the stagnation region where a spurious overproduction of kinetic energy is observed, see figure 3.4), but the length scale predicted by the $\varphi - f$ model equipped with the time-scale limiter is well above the equilibrium length scale in the region $y_+ \leq 100$ and at the same time correctly predicts the secondary peak in the Nusselt number distribution. It turns out that the length scales in boundary layers subjected to any pressure gradient cannot admit equilibrium log-layer scaling. Regarding the favorable pressure gradient, the channel flow boundary layer ($Re_\tau = 395$) is somewhat analogous to the boundary layer in the stagnation region of the impinging jet, although the pressure gradient is much stronger in the latter case. No stagnation anomaly or spurious pro-

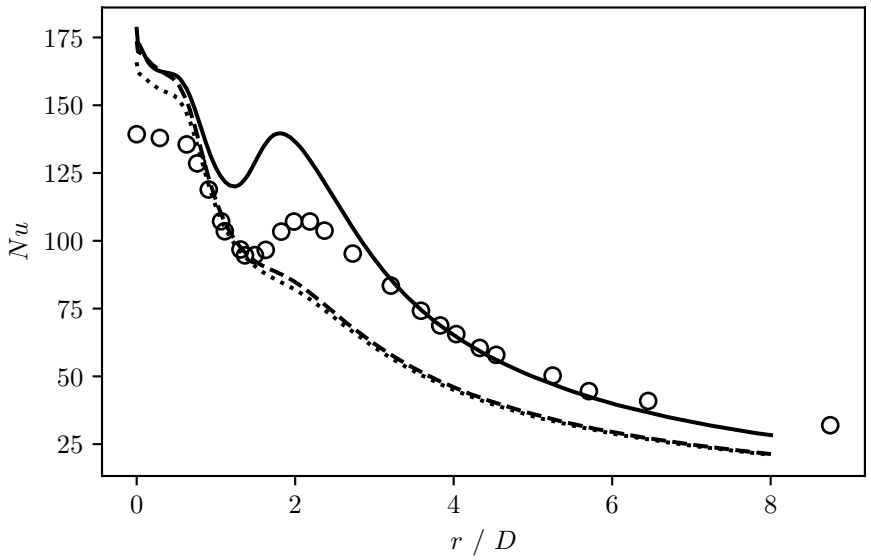

Figure 3.8: Nusselt number distributions obtained by applying various modifications to $\varphi - f$ model. —— Kato - Launder modification; - - - - Yap correction; ····· "differential" Yap correction (3.13) ○ Baughn et. al (1989), $Re = 23750$.

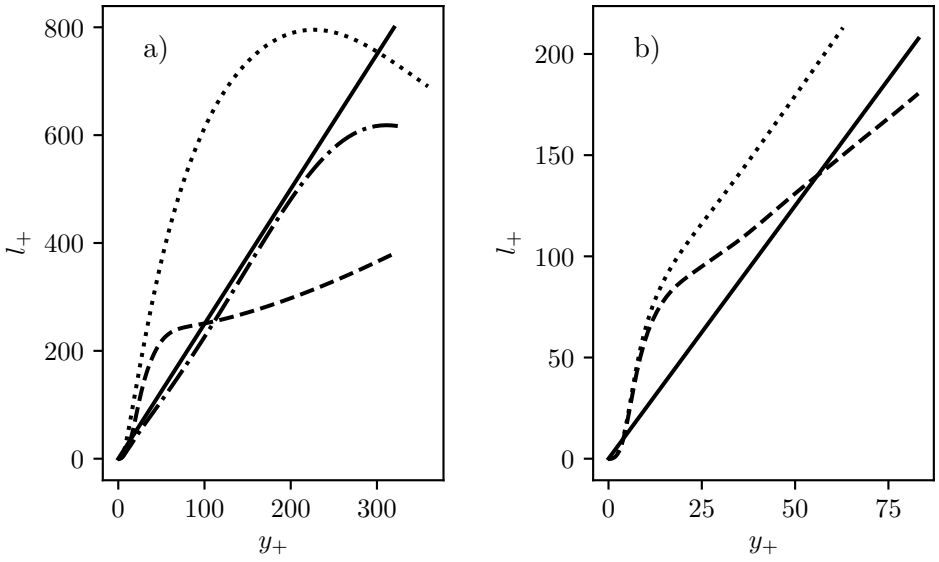

Figure 3.9: a) Length scale profiles at r/D = 0.5 of the plate computed by $\varphi - f$ model with various modifications. - - - - time-scale limiter, C_{lim} = 0.5; ····· no modification applied; —·—· Yap correction. b) Length scale profiles obtained from DNS databases. - - - - turbulent channel flow, Re_τ = 395 [1]; zero pressure gradient boundary layer, Re_θ = 4060 [6]; Both figures: —— equilibrium length scale l_e.

duction of kinetic energy can be observed in channel flow computations, but the Yap correction term could still spuriously penalize the excessive values of the length scale in terms of the equilibrium one, even when this is a natural occurrence when the pressure gradient is present. The complete disregard for the pressure gradient in the log-layer scaling is behind the author's objection against the Yap correction. As the computed length scales are driven to the equilibrium one derived from log-layer assumptions omitting the pressure gradient, the $\varphi - f$ model gets desensitized to the strongly favorable pressure gradient, hence it cannot capture the effect that the pressure gradient exerts on the boundary layer.

The author further proposes that any modification designed to suppress stagnation point anomalies should remove some obvious errors, such as the overproduction of turbulence kinetic energy extending far above the boundary layer in the stagnation region observed in figure 3.4, which is intimately linked to the formula $2\nu_T|S|^2$ breaking down. Although this is more a visual clue than a proper validation done by examining the predicted heat transfer rates, one can still find out if the mechanism of the modification targets the underlying issue by simply looking at the predicted kinetic energy field. The Yap correction fails at the removal of the kinetic energy "bubble" near the jet

centerline, hence the predicted kinetic energy field looks like the one in the left figure 3.4. This fact indicates that Yap correction was never designed to treat stagnation point anomalies and was misused in the present case. Perhaps the author's scrutiny of the term is not completely justified.

The right figure 3.9 also shows an example of a length scale (at the point where the momentum thickness Reynolds number $Re_\theta = 4060$) occurring in the developing zero pressure gradient boundary layer. As can be readily observed, the slope of the length scale is very similar to the slope of the equilibrium log-layer scaling in the region $y_+ > 25$ (actually, the length scale is approximately linear up to $y_+ \approx 200$). That's not surprising, as real zero pressure gradient boundary layers (where Clauser's parameter $\beta_T \approx 0$) are very close to the idealized state of the equilibrium boundary layer. Thinking in terms of the slopes of turbulence length scales rather than their values motivates a sort of "differential" Yap correction term, presented as:

$$S_{diff\varepsilon} = \max\left[\left(\frac{|\nabla l|^2}{C_\mu^{-1.5}\kappa^2} - 1\right)\left(\frac{l}{l_e} - 1\right)\left(\frac{|\nabla l|^2}{C_\mu^{-1.5}\kappa^2}\right)\frac{\varepsilon}{T}, 0\right]. \tag{3.13}$$

The driving vehicle of this term is the ratio of the inner product of the length scale gradients $\nabla l.\nabla l$ to the squared slope of the equilibrium length scale. The expression $(l_e/l - 1)$ was kept the same as in the original Yap correction term, combined with maximum function, which will again constrain the effects to the near-wall region. The expression containing the excess of the squared length scale to the squared slope of the equilibrium length scale was also added to suppress the term whenever the length scales align. Surprisingly, the newly proposed term produces almost the same result as the original Yap correction, as the figure 3.8 shows.

The newly introduced term requires further examination so that its qualitative nature can be revealed. Substituting the definitions $l = k^{1.5}/\varepsilon$, $T = k/\varepsilon$ to the product $|\nabla l|^2\varepsilon/T$ yields the expression:

$$\frac{\varepsilon^2}{k}\frac{\partial\left(k^{1.5}/\varepsilon\right)}{\partial x_j}\frac{\partial\left(k^{1.5}/\varepsilon\right)}{\partial x_j},$$

which can be expanded as:

$$\frac{9}{4}\frac{\partial k}{\partial x_j}\frac{\partial k}{\partial x_j} - 3\frac{k}{\varepsilon}\frac{\partial k}{\partial x_j}\frac{\partial \varepsilon}{\partial x_j} + \frac{k^2}{\varepsilon^2}\frac{\partial \varepsilon}{\partial x_j}\frac{\partial \varepsilon}{\partial x_j}. \tag{3.14}$$

That's a significant revelation - these expressions are recognized as so-called cross-diffusion terms (to be exact only the term $\partial k/\partial x_j \partial\varepsilon/\partial x_j$ can be regarded as cross-diffusion, it involves both k and ε; author chooses to call combinations of such coupled gradient terms as cross-diffusion because their qualitative behavior is similar). Cross diffusion arises when the original transport equation for the specific dissipation frequency ω is rewritten as an ε equation by

employing the substitution $\varepsilon = C_\mu k\omega$:

$$\frac{\mathrm{D}\varepsilon}{\mathrm{D}t} = \frac{C'_{\varepsilon 1}\mathcal{P}_k - C'_{\varepsilon 2}\varepsilon}{T} + \frac{\partial}{\partial x_j}\left[\left(\nu + \frac{\nu_T}{\sigma_\varepsilon}\right)\frac{\partial \varepsilon}{\partial x_j}\right] - 2\left(\nu + \frac{\nu_T}{\sigma_\omega}\right)\frac{\partial k}{\partial x_j}\frac{\partial\left(\varepsilon/k\right)}{\partial x_j}. \quad (3.15)$$

The equation written above reproduces the standard ε equation, the exact expressions for the transformed coefficients $C'_{\varepsilon 1}$ and $C'_{\varepsilon 2}$ are not important at the moment. The extra source term is the aforementioned cross-diffusion.

Wilcox [24, Sec. 4.6] argues that the absence of cross-diffusion in the ε equation is the reason behind the general overprediction of skin friction coefficients and poor predictions of adverse pressure gradient boundary layers. The arguments come from perturbation analysis of self-similar defect layer equations (with $\beta_T = const.$, note that keeping $\beta_T \approx const.$ with a non-zero pressure gradient is tough even when the flow is simulated). The poor performance of the $k-\varepsilon$ model was explained by analyzing the perturbation solutions formally matched to the law of the wall (log-layer scaling). For the turbulence length scale l, it was found that it behaves according to (η is a wall-normal coordinate in defect-layer scaling):

$$l \sim A\eta + B\beta_T\eta^2 \ln\eta + \ldots \ as \ \eta \to 0.$$

The second term proportional to β_T is interesting, as it turns out the $k-\varepsilon$ model computes the values of the multiplicative constant B much larger than the $k-\omega$ model, thus for the adverse pressure gradient, the $k-\varepsilon$ models' turbulence length scales tend to be too large. The net effect of cross-diffusion is apparently to suppress the rate of increase of l close to the surface. This notion coincides with what the Yap correction tries to achieve, to ultimately drive the turbulence length scale closer to the log-layer scaling in the presence of adverse pressure gradients. So the net effect of adding the Yap correction term to the ε equation should be similar to that of cross-diffusion, at least for this case. The Yap correction was designed to improve predictions of low-Reynolds number $k-\varepsilon$ models (employing viscous damping functions of van Driest type, a most prominent example is Launder-Sharma model [32]), which don't work well for flows with adverse pressure gradients. This combination can indeed be effective, as the following comparative study shows [33].

3.4.4 Introducing pressure gradient to the dissipation rate equation

The upcoming subsection was motivated by an article [34], where an additional term was added to the dissipation rate equation, in the hope of improving predictions of $k-\varepsilon$ model for the two-dimensional adverse pressure gradient boundary layers. Omitting a relatively short, but confusing derivation, the final form of the additional term reads (in this context, U is the x-component of the mean velocity):

$$-C'_{\varepsilon 3}\frac{k}{T}\frac{\partial U}{\partial x}. \quad (3.16)$$

In an adverse pressure gradient boundary layer, $\partial U/\partial x < 0$ (the fluid is decelerating), this term is positive, therefore enhancing the dissipation rates. Although the connection is somewhat loose, this term ultimately introduced the author to the idea of combating the stagnation point anomaly by enhancing the dissipation rates with terms proportional to the acceleration of the fluid in the direction of the velocity itself. Based on the term (3.16), a more general term can be proposed, which encapsulates the aforementioned idea of penalizing the acceleration in the direction of the velocity:

$$+C'_{\varepsilon 3}\frac{k}{T}\left|\frac{\partial U_i}{\partial x_j}r_j r_i\right|, \tag{3.17}$$

where r_i stands for component of the normalized velocity vector $U_i/|U|$, hence it is a unit vector. The double contraction of the mean velocity gradient with the unit vectors extracts a scalar value, which can be thought of as the acceleration of the fluid along the streamlines. This product can be both positive or negative, depending on whether the fluid is accelerating or decelerating in the direction of velocity. The magnitude of this scalar value was used, to enhance the dissipation rate in both cases. Figure 3.10 shows, that the term (3.17) can alleviate the stagnation point anomaly. Approaching the plate from above, the fluid rapidly decelerates, hence the formula $2\nu_T|S|^2$ overestimates the production rate of kinetic energy and the dissipation rate equation is in imbalance, the term (3.17) counters this effect by enhancing the dissipation rate in the same regions where the strain rates are large. The value of $C'_{\varepsilon 3} = 1.44$ was used in accordance with the article [34], although one can see that a general calibration would be difficult.

Let's not worry too much about the performance of the newly proposed term, instead let's design a modification of the ε equation that on top of dealing with the stagnation anomaly, can capture the strongly stabilizing effects of the pressure gradient in the region close to the jet centerline. Consider a plane boundary-layer flow over a smooth surface, then the equation describing irrotational inviscid flow above the boundary layer may be approximated as [35]:

$$U_o\frac{\mathrm{d}U_o}{\mathrm{d}x} = -\frac{\mathrm{d}P_o}{\mathrm{d}x},$$

where U_0 is a component of velocity in the streamwise direction (subscript "o" denotes outside). Even though this is not necessarily related to the case at hand, the equation written above sums up how the pressure gradient is related to the acceleration of the fluid far away from the walls.

A handful of terms involving pressure gradient can be formed that are dimensionally consistent with the ε equation, but the following one aligns the best with the idea of enhancing dissipation rates when large acceleration in the streamwise direction is encountered:

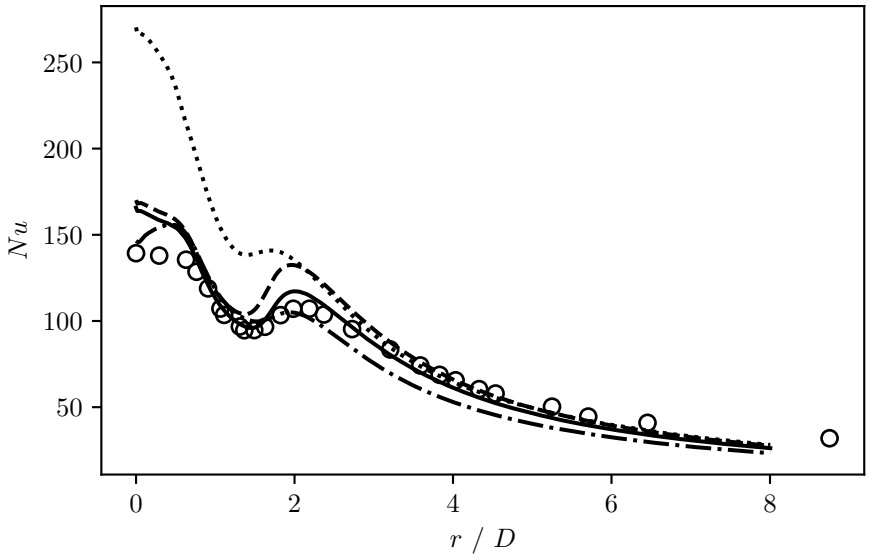

Figure 3.10: Nusselt number distributions obtained by applying various additional terms to ε equation, computed by $k-\varphi$ model. - - - - pressure gradient term (3.18) $C_p = 0.15$; —— pressure gradient term + time-scale gradient term (3.19) $C_p = 0.15, C_{\varepsilon T} = 0.035$; —·—· velocity gradient term (3.17) $C'_{\varepsilon 3} = 1.44$; ····· no additional term applied ; ○ Baughn et. al (1989), $Re = 23750$.

$$+C_p \frac{\sqrt{k}}{T} \left| \frac{\partial P}{\partial x_i} r_i \right|. \tag{3.18}$$

Note the dependence of both terms (3.17, 3.18) on k. It's one of the reasons why the subsequent computations with these modifications are convergent. Since both terms are designed to counteract the overproduction of the kinetic energy in the stagnation region, they are also large there. Thus they enhance the dissipation rate, which in turn dissipates the kinetic energy, and the dissipation rate is consequently diminished (production rate is a source in ε equation). Both terms will rescale themselves according to this mechanism, thus never disrupting the balance of the ε equation. Consider adding a term proportional to $(\partial P/\partial x_i)^2$. It will always have the same values in the stagnation region, irrespective of the value of a multiplicative constant.

Figure 3.10 shows that this term is also effective against the stagnation point anomaly, the pressure-gradient term enhances the dissipation rates only where the pressure-gradient is present, so the location of the laminar-to-turbulent transition is predicted quite accurately, however, the secondary peak occurring in the Nusselt number distribution is grossly overpredicted. Regarding the value of C_p, it was found by simple trial and error that the reasonable bounds are $0.1 \leq C_p \leq 0.2$.

Note that these ad hoc modifications are not theoretically justified and appropriate values of multiplicative constants depend on the case at hand. A high degree of a posterioriness associated with the use of the additional terms is embarrassing. Both the velocity gradient and pressure gradient terms serve the purpose to show the reader that the root cause of the stagnation anomaly can be counteracted directly by increasing the dissipation rates proportionally to the fluid's streamwise acceleration. It is a purely balancing approach motivated by simple observations, there is no turbulence modeling involved.

3.4.5 Exploring the possibility of adding cross-diffusion to the ε equation without blending functions

The succeeding subsection is devoted to a simple demonstration of how the coupled gradient terms such as the ones in (3.14) can be added to the ε equation to enhance dissipation rates in the near wall regions. To motivate the approach assumed by the author, let's have a look at more theoretically "justified" ways to add such terms to the ε equation. The extra source term in equation (3.15) can be regarded as a "failing link" between the $k-\varepsilon$ and $k-\omega$ model, so perhaps including some appropriate fraction of cross-diffusion could improve the predictions of the model. But this new "hybrid" model may partially inherit the sensitivity of the predictions to the freestream value of ε, which is undesirable. Another way to generalize the ε equation is to derive diffusion terms utilizing some elaborate theory, for instance, two-scale direct-interaction approximation. Yoshizawa [36] used the results of the theory to introduce additional terms to the ε equation:

$$\frac{\partial}{\partial x_j}\left(C_{kk}k\frac{\partial k}{\partial x_j}\right)+C_{k^2}\frac{\partial k}{\partial x_j}\frac{\partial k}{\partial x_j}+C_{k\varepsilon}\frac{k}{\varepsilon}\frac{\partial k}{\partial x_j}\frac{\partial \varepsilon}{\partial x_j}+C_{\varepsilon^2}\frac{k^2}{\varepsilon^2}\frac{\partial \varepsilon}{\partial x_j}\frac{\partial \varepsilon}{\partial x_j}$$

Well, it's nice that the inclusion of the coupled gradient terms in the ε equation can be theoretically justified. But the delusion of added rigor falls flat once one realizes that the multiplicative constants are not fixed by the theory and are hard to calibrate. The dilemma of the additional closure coefficients is encountered again and in this case, the level of arbitrariness is downright bizarre. The reader can learn about such generalized $k-\varepsilon$ models in a summary of two-equation eddy viscosity models [37]. The author of the report himself questioned the vast discrepancies between the models - the values of constants being of markedly different orders and even worse, signs of the coupled gradient terms differing for each model.

Inclusion of coupled gradients is even more problematic in terms of numerical tractability. In the report [38], authors devised fairly successful source terms for boundary layer flows involving gradients of kinetic energy, but these uniformly led to disastrous results in free shear flows. Indeed, such terms are large even far away from the walls, disrupting the balance of the ε equation

and can even cause instabilities. One could argue that we also need to re-calibrate the coefficients $C_{\varepsilon 1}, C_{\varepsilon 2}$, but managing other two or three closure coefficients multiplying the coupled gradient terms at the same time would be strenuous. To circumvent these difficulties, one would have to design a blending function, to switch off the coupled gradients outside the boundary layer.

The problem of numerical robustness and too many free closure coefficients can be taken care of. Instead of adding individual coupled gradient terms to the ε equation, we should consider gradients of quantities, which experience a substantial rate of change in the boundary layer and then vary steadily, hence the additional source term will be much smaller outside the boundary layers. Immediately, the turbulence length scale l and time scale T come to mind. The source term $|\nabla l|^2 \varepsilon / T$ (introduced in the "differential" Yap correction (3.13)) expanded in (3.14) involves the coupled gradients, is always positive and the individual coefficients are set apriori. Thus only one constant is needed to multiply the whole expression, instead of three. A source term involving an inner product of the time-scale gradient sharing these attractive qualities can be also devised:

$$+C_{\varepsilon T} k \frac{\partial T}{\partial x_j} \frac{\partial T}{\partial x_j} \frac{\varepsilon}{T}. \tag{3.19}$$

Since the product $k(\nabla T)^2$ is dimensionless, we can reason about adding the term (3.19) to the dissipation equation as decreasing the sink term or the "generalized" $C^*_{\varepsilon 2}$ constant:

$$C^*_{\varepsilon 2} \frac{\varepsilon}{T} \;=\; \left(C_{\varepsilon 2} - C_{\varepsilon T} k \frac{\partial T}{\partial x_j} \frac{\partial T}{\partial x_j} \right) \frac{\varepsilon}{T}. \tag{3.20}$$

The $k-\varepsilon$ model is sensitive to the value of the difference $C_{\varepsilon 1} - C_{\varepsilon 2}$, so even a modest reduction of $C_{\varepsilon 2}$ can result in big qualitative changes of the model's behavior. Value of the constant $C_{\varepsilon T}$ can be of order 10^{-2} and the near-wall dissipation rates are notably increased, namely in the region of the secondary peak, as we can see in figure 3.10. The aforementioned term was used in conjunction with the pressure gradient one. The value $C_{\varepsilon T} = 0.015$ was again obtained a posteriori by simple trial and error.

The addition of the term involving gradients of the time scale ratio to the ε equation can be used to formulate a more general $k-\varepsilon$ model. Let's shed some light on the process of calibration. Firstly, consider rewriting the term (3.19) to the form:

$$C_{\varepsilon T} \nu_T \left(\frac{\partial k}{\partial x_j} \frac{\partial k}{\partial x_j} - \frac{2}{k} \frac{\partial k}{\partial x_j} \frac{\partial \varepsilon}{\partial x_j} + \frac{1}{\varepsilon} \frac{\partial \varepsilon}{\partial x_j} \frac{\partial \varepsilon}{\partial x_j} \right).$$

This formulation can be used to study the behavior of the newly developed model near the outer edges of shear layers. A permissible range of values for $C_{\varepsilon T}$ and perhaps new values for constants $\sigma_k, \sigma_\varepsilon$ would have to obey the

constraints for the analytic solution of the idealized edge problem. Explicit solutions of these ordinary differential equations can be derived in the same manner as in the article [39], note that inclusion of the term $(\nabla k)^2$ will greatly complicate the analysis. The next step would be to recalibrate the coefficients $C_{\varepsilon 1}, C_{\varepsilon 2}, C_{\varepsilon T}$ as usual, by matching the measured spreading rates for free shear flows - far wake, mixing layer, plane jet, round jet ...That perhaps wouldn't be that time consuming, because these flows are considered self-similar and approximations of the corresponding equations reduce to ordinary differential equations. Validation should also be done on other canonical flows, such as channel flows and zero-pressure boundary layers. A similar model recalibration was done by Hellsten in his doctoral thesis [40]. Well, the introduction of a new two-equation scale-determining model is clearly beyond the scope of this thesis.

3.5 Note on a nonexistent transition predicted by $k-\omega$ models

The absence of the secondary peak in the predicted Nusselt number distribution of the $k-\omega$ model was already discussed in section 3.3. The author's proposal of a possible solution to this problem does not consist in applying any ad hoc modifications, as was done in the case of the $\varphi - f$ model. Because both Wilcox's $k-\omega$ model and the updated version of the $k-\omega$ SST model from 2003 [41] already use eddy viscosity limiters analogous to the realizability constraints. The matter of whether the author even uses implementations of these models consistent with the official formulations will be discussed in section 4.3.

The question of transition can be treated in the framework of linear eddy viscosity models (namely $k-\omega$ ones). One of the ways to tackle the problem is to develop a transport equation for the so-called intermittency function γ (intermittency - the fraction of time that the flow at any point is turbulent, rises from zero to unity during transition) and modulate with it either eddy viscosity or the production term in the k equation. Most linear eddy viscosity models predict the transition very early, so ν_T will reach turbulent levels, and $\gamma\nu_T$ will rise under the control of γ. Coupling a transitional model to a $k-\omega$ model is very common. An example of such a model is the $\gamma - SST$ model, intricate details of the equations, correlations, and model constants are omitted for the sake of brevity. The reader can refer to the article introducing the model [42].

The predicted heat transfer rates by the $\gamma - SST$ are in excellent agreement with experimental in both the stagnation and transition region, as figure 3.11 shows. This is a success, albeit achieved at a rather high price. A far more elaborate model had to be used when compared to the standard $k-\omega$ SST model. Little side note on how this result was achieved computationally: a

converged solution obtained by the $k-\omega$ model was used as an initial condition. In this way, the previously mentioned problems with entrainment and reentering of the fluid into the domain through outlet boundaries were not present anymore. Thus simple homogenous Neumann boundary conditions for the intermittency function γ could be used at the outlet boundaries.

3.6 Profiles of mean velocity and Reynolds shear stress

Profiles of mean velocity and Reynolds shear stress at various distances from the jet axis are shown in figures 3.12 and 3.13. The predictions of the listed models are kind of all over the place in the case of Reynolds shear stress profiles, the only thing one can surely say is that Wilcox's $k-\omega$ is in good agreement with the experimental data for the stations $r/D = 2.5$ and $r/D = 3$. On the other hand, an important conclusion can be drawn from the velocity profile predictions. Both Wilcox's $k-\omega$ model and $\varphi - f$ with the time scale limiter overpredict the peaks in velocity profiles for stations $r/D = 2.5, 3$; the cause of this issue lies in increased overall dissipation rates ($k-\omega$) and limited eddy viscosity ($\varphi - f$ with the time scale limiter). As the eddy viscosity is suppressed in near-wall regions in both cases, the velocity profiles are less "diluted" by turbulent mixing resulting in overpredicted peaks. The $\varphi - f$ model with no realizability constraints provides more reasonable predictions of

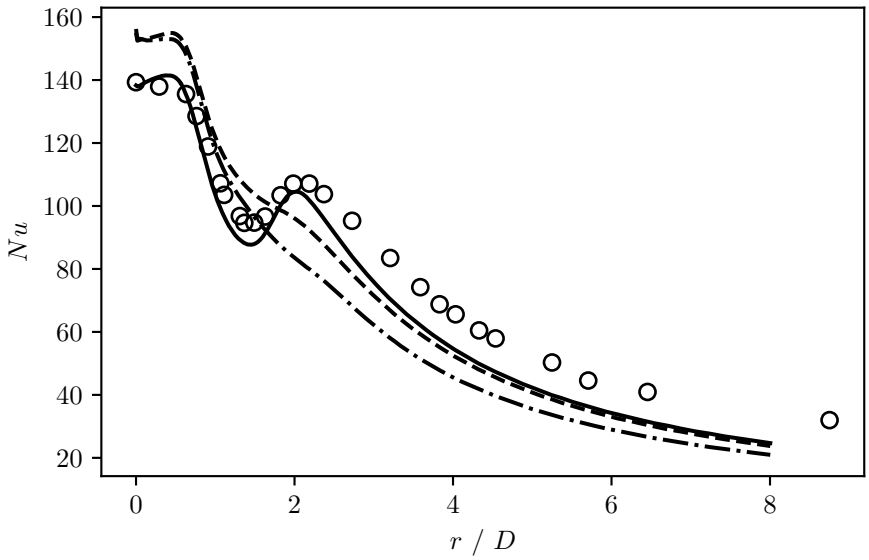

Figure 3.11: Predicted Nusselt number distributions by various eddy viscosity models. –·–· Wilcox's $k-\omega$ 2006 model; - - - - $k-\omega$ SST model; —— $\gamma-SST$ model; ○ Baughn et. al (1989), $Re = 23750$.

velocity profiles, but at the same time, the model grossly overpredicts Nusselt numbers in the stagnation region. The time-scale limiter certainly improves the predictions of heat transfer rates, but lower near-wall eddy viscosity levels are not favorable for all the quantities of interest.

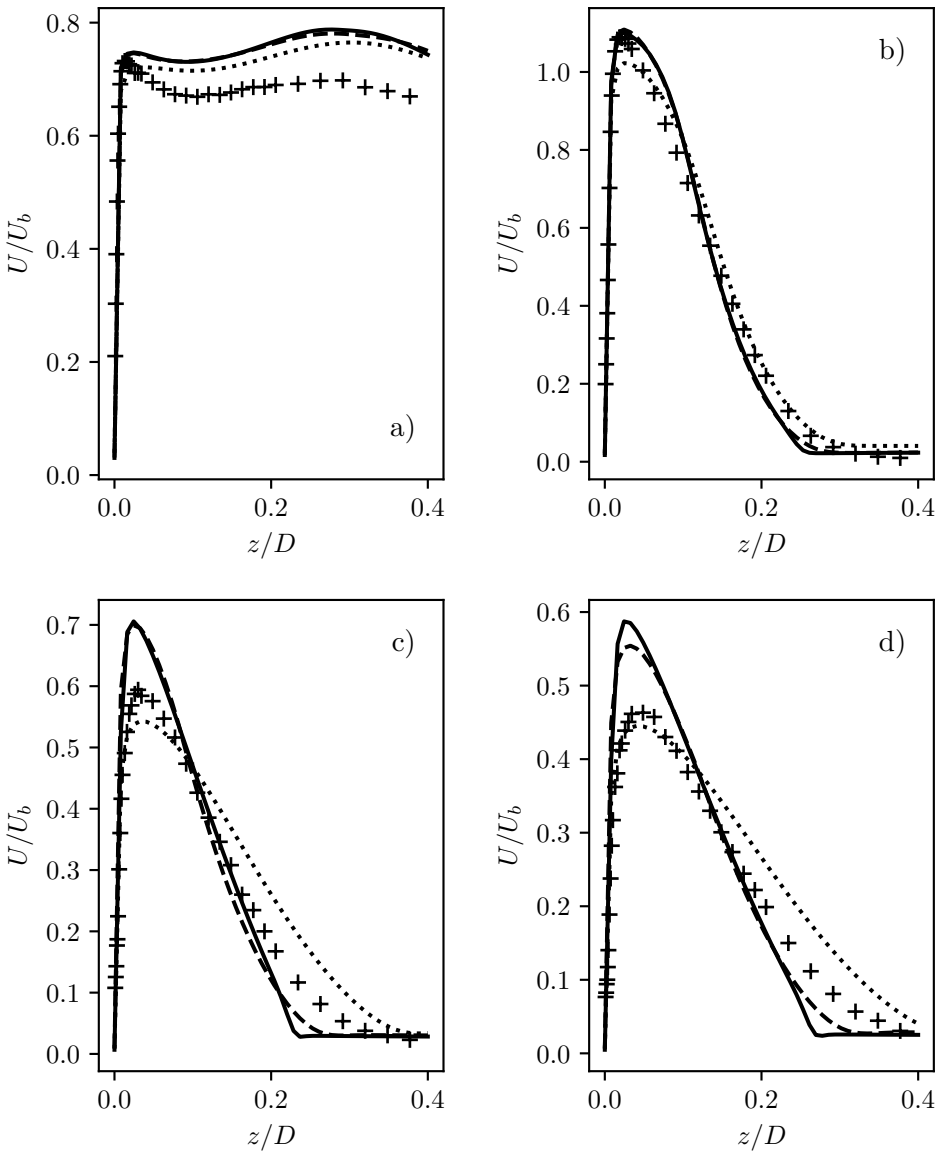

Figure 3.12: Computed profiles of mean velocity. a) Station $r/D = 0.5$; b) Station $r/D = 1$; c) Station $r/D = 2.5$; d) Station $r/D = 3$; ····· $\varphi - f$ without modifications, - - - - $\varphi - f$ with time-scale limiter, $C_{lim} = 0.5$; —— Wilcox's $k - \omega$ 2006 model; + ERCOFTAC experimental data [3].

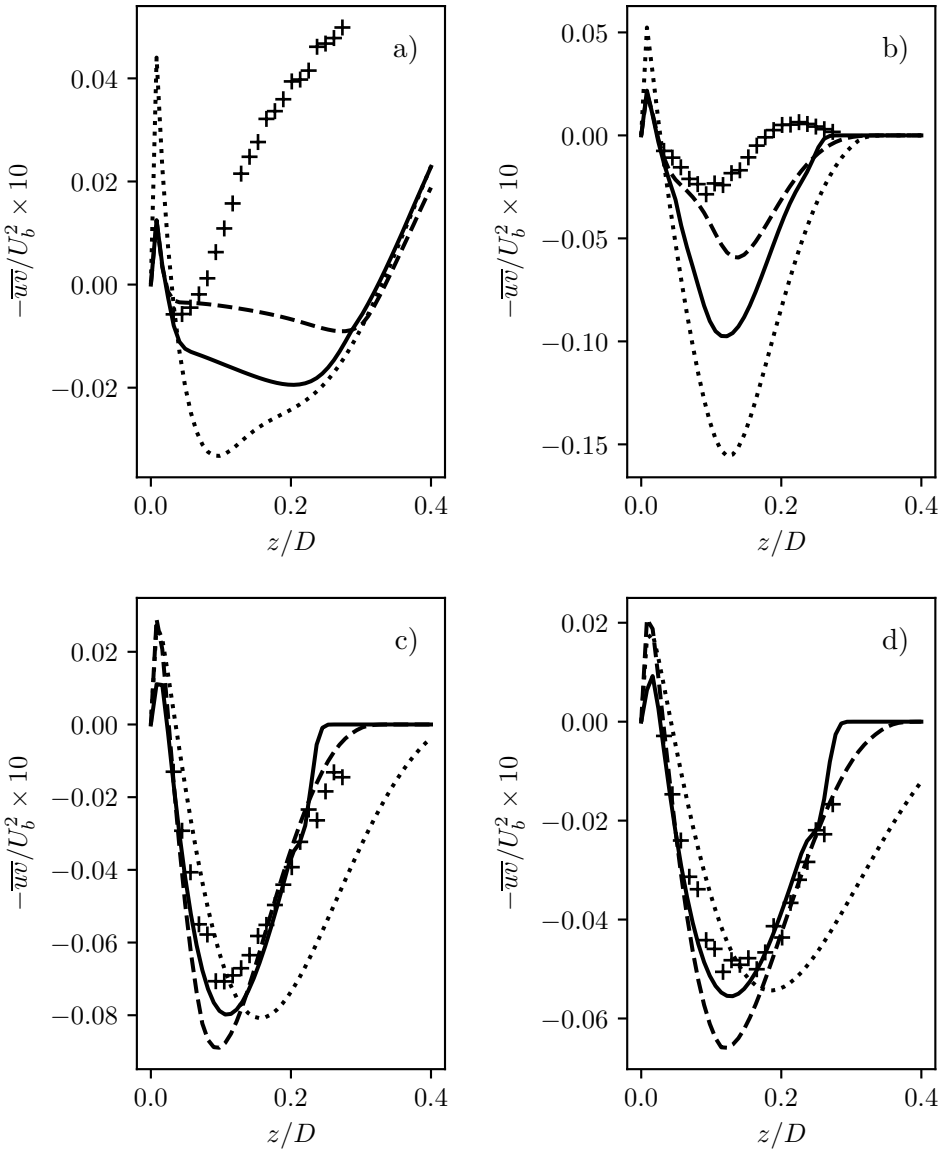

Figure 3.13: Computed profiles of Reynolds shear stress.a) Station $r/D = 0.5$; b) Station $r/D = 1$; c) Station $r/D = 2.5$; d) Station $r/D = 3$; ····· $\varphi - f$ without modifications, - - - - $\varphi - f$ with time-scale limiter, $C_{lim} = 0.5$; —— Wilcox's $k - \omega$ 2006 model; + ERCOFTAC experimental data [3].

3.7 Nusselt number predictions for the case $H/D = 6$

Nusselt number distributions were also computed for the nozzle-to-plate spacing $H/D = 6$ (same $Re_b = 2.3 \times 10^4$). The geometry of the domain and grid is

analogous to the case $H/D = 2$. Boundary conditions were set in the same way as in the previous case. A grid refinement study was done for this case too, the results and the choice of the appropriate grid are listed in the appendix A.1.

We can assess the performance of various modifications applied to the $\varphi - f$ model in figure 3.14. The Kato-Launder modification seems to perform the poorest, the overprediction of Nusselt numbers is analogous to the $H/D = 2$ case. The time-scale limiter and additional terms applied to the ε equation are quantitatively in pretty good agreement with the experimental data. In terms of qualitative agreement, things are a little bit complicated. Note that a strong favorable pressure gradient is present in the region $0 \leq r \leq 2D$ even in this configuration and the $\varphi - f$ model seems to be still sensitive to it. Thus it tends to form mild secondary peaks, which is certainly incorrect, as it was noted in section 3.1, Nusselt numbers should monotonically decrease. The secondary peak is more pronounced when an additional velocity gradient term (3.17) and pressure gradient term (3.18) is added to the ε equation, but that is understandable since both terms are closely related to the pressure gradient. On the other hand, the Yap correction is now the modification that can provide qualitatively correct results, as can be seen in figure 3.15. It was hypothesized, that Yap correction has a similar effect on the ε equation as cross-diffusion and significantly desensitizes the model to favorable pressure gradients. Note this was disadvantageous in the $H/D = 2$ case. The results produced by both $k-\omega$ models support the idea because they are indeed very similar. Perhaps the overall best result was obtained by the $k-\omega$ SST model.

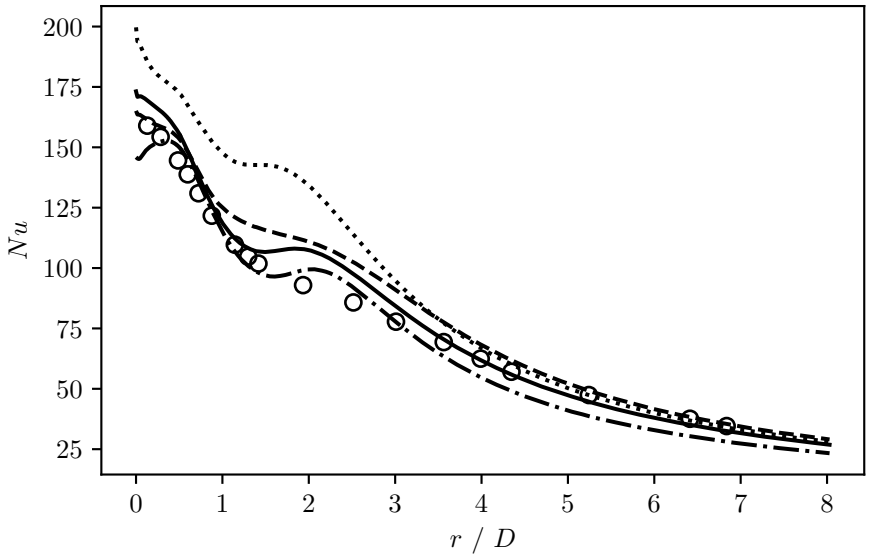

Figure 3.14: Predicted Nusselt number distributions by $\varphi - f$ model employed with various modifications. −·−· velocity gradient term (3.17), $C'_{\varepsilon 3}$; - - - - time-scale limiter, $C_{lim} = 0.5$; —— pressure gradient term (3.18) and time-scale gradient term (3.19), $C_p = 0.15, C_{\varepsilon T} = 0.035$; ····· Kato-Launder modification; ○ Baughn et. al (1989), $Re = 23\,750$.

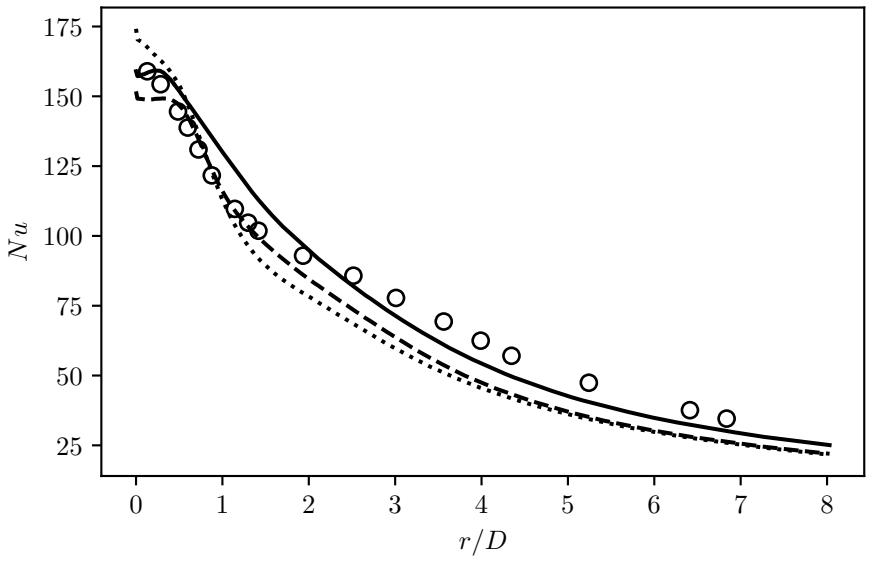

Figure 3.15: Predicted Nusselt number distributions two $k - \omega$ models and $\varphi - f$ model with Yap correction. - - - - Wilcox's $k - \omega$ 2006 model; —— $k - \omega$ SST model; ····· $\varphi - f$ model with Yap correction; ○ Baughn et. al (1989), $Re = 23\,750$.

Chapter 4

2D infinite serpentine passage

In the following chapter, a particular flow configuration will be considered - a 2D infinite serpentine comprised of two 180° U-bends, where a separation of the flow occurs. The discussion will be primarily concerned with the $\varphi - f$ model with realizability constraints applied, namely the time-scale limiter. Firstly, out of all modifications presented in this thesis, the realizability constraint makes the most sense from a theoretical standpoint - the bound $0 \leq \overline{u_i^2} \leq 2k$ keeps the normal stresses in the physically permissible range. Imagine a simulation of a stationary turbulent flow modeled by a turbulence model, which predicts $0 > \overline{u_i^2}$, then the simulation cannot possibly correspond to some real statistically stationary process. This a serious issue and a realizability constraint can prevent it. Secondly, the time-scale limiter can effectively suppress stagnation anomalies, as we have seen in the case of an impinging jet. Thus relevant questions arise. Can we apply a time-scale limiter to any flow configuration? Will the multiplicative constant C_{lim} = 0.5, enhancing the limiter's effect, always yield appropriate results?

In this flow configuration strong streamline curvature effects are present. The scalar eddy viscosity models are based on transport equations for scalar quantities k, ε, ω ...By their scalar nature, the models do not respond appropriately to the streamline curvature, because it affects individual components of the Reynolds stress tensor. No curvature corrections were considered for the $\varphi - f$ $(k-\omega)$ model. The results certainly won't be in very good agreement with the data, but still, the question of the appropriateness of the time-scale limiter for flows with no apparent stagnation regions is valid.

4.1 Computational setup and boundary conditions

This flow configuration was based on the steady case in the DNS of Laskowski and Durbin [7]. The geometry of the domain with highlighted measuring stations for the velocity profiles is shown in figure 4.1. Since the geometry is symmetric around the horizontal channel joining the two 180° bends, the

obtained results were validated only in the upper U-turn. Unfortunately, the precise dimension of half channel width is not available, so the author used the value of $\delta = 0.019\,05\,\mathrm{m}$. Consequently, the inner radius had a value of $r_i = 0.019\,05\,\mathrm{m}$ and outer $r_o = 0.057\,15\,\mathrm{m}$.

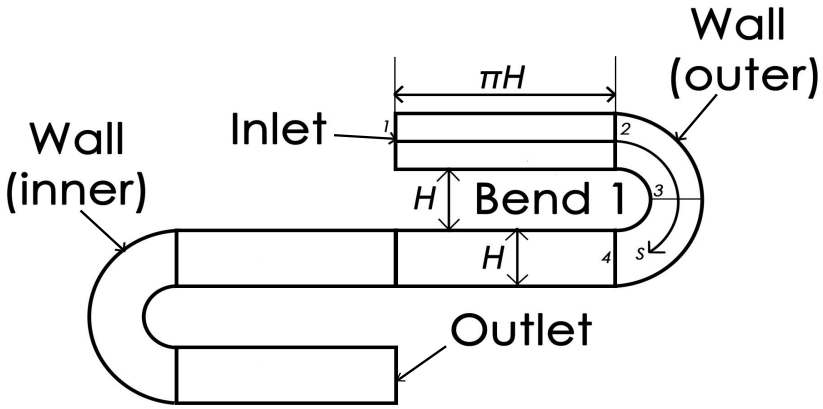

Figure 4.1: Sketch of the geometry of the domain with measuring stations (numbers). H corresponds to the channel width, consequently half-channel width is $\delta = H/2$. The arc-coordinate s has its origin in station 1.

Authors have chosen an infinite passage to obtain DNS data independent of the inlet conditions. Thus, for quantities $U_i, k, \varphi, \varepsilon, \omega, f$ periodic boundary conditions were set for both inlet and outlet. Setting boundary conditions for pressure is a little bit more involved because a pressure drop ΔP has to be set between the inlet and the outlet, written precisely as

$$P_{inlet} = \Delta P + P_{outlet}, \tag{4.1}$$

so that the actual flow through the passage develops. Reynolds number based on half channel width δ and bulk velocity U_b was 5600. To set the desired bulk velocity in accordance with the Reynolds number, a simple scheme was constructed to iteratively update the pressure drop. The author assumed that the pressure drop is proportional to the square of the bulk velocity, hence $\Delta P \propto K U_b^2$. The scheme consists of three updates at every iteration of the

SIMPLE algorithm:

$$\begin{aligned} K^n &\coloneqq \frac{\Delta P^{n-1}}{\left(U_b^n\right)^2}; \\ \Delta P^n &\coloneqq K^n \left(U_b^*\right)^2; \\ \Delta P^{n-1} &\coloneqq \Delta P^n; \end{aligned}$$

The symbol U_b^* denotes the target bulk velocity calculated from the Reynolds number. The superscripts n and $n-1$ refer to the current and previous iterations. This scheme is rather simple and prone to oscillations. Sometimes it was necessary to prescribe a fixed pressure drop at the start of the iteration procedure and iterate until at least some flow rate through the serpentine developed and then the scheme was applied to correct the pressure drop. The author also experimented with under-relaxation and less frequent updates of the pressure drop but ultimately found out that the scheme converges to the desired pressure drop if it is updated at every iteration of the SIMPLE algorithm and no under-relaxation is applied.

The treatment of solid boundaries was the same as in the case of the impinging jet. Homogenous Dirichlet boundary conditions were prescribed for the quantities k, φ, f, U_i and homogenous Neumann boundary conditions for pressure P. Values for ε, ω were again obtained from the limiting formulas (1.7), (3.3) evaluated at the center of cells adjacent to the walls.

A grid refinement study was done for this case too, the results and choice of the appropriate grid are available in the appendix A.2.

4.2 Discussion of the results

The predicted data that shall be validated are mean velocity profiles at the measuring stations 1-4 (figure 4.1) and skin friction coefficient distributions along the inner and outer walls of the upper U-bend. The skin friction coefficient in this case is defined with the formula:

$$c_f = 2\frac{\tau_w}{U_b^2}.$$

The reader shall be noted that the data for mean velocity from the DNS as presented here, are scaled by the bulk velocity U_b and not by friction velocity u_τ. Since the pressure drop was always set in such a way as to reach the target bulk velocity at the inlet (or outlet), bulk velocity scaling is more natural. Fortunately, both Reynolds numbers $Re_b = 2\delta U_b/\nu = 5600$, $Re_\tau = \delta u_\tau/\nu = 180$ are available. The DNS data were multiplied by the ratio $u_\tau/U_b = 2Re_\tau/Re_b$ to achieve the same normalization.

Since the case is now fully 2D, the 2D variant of the realizability constraint was used, so the constant C_{lim}^{2D} now equals $C_{lim}^{2D} = 2C_{lim}/\sqrt{3}$. Plugging in

the value of $C_{lim} = 0.5$, yields $C_{lim}^{2D} \approx 0.577\,35$, this value was used for all the applications of a realizability constraint to the $\varphi - f$ model.

Model	Sep.	Reatt.	Len.
DNS	10.731	14.347	3.616
$\varphi - f$	11.493	14.004	2.511
$\varphi - f$ + stress limiter	10.31	16.021	5.711
$\varphi - f$ + time-scale limiter	9.954	17.441	7.487
$k - \omega$, no stress limiter	10.562	15.784	5.22
$k - \omega$ + stress limiter	10.131	16.542	6.411
$k - \omega$, inconsistent impl.	9.818	18.704	8.886

Table 4.1: Predicted separation points (Sep.), reattachment points (Reatt.), and recirculation lengths (Len.) in 2D infinite serpentine. Quantities are expressed as multiples of half-channel width δ.

First mildly anxiety-inducing fact is that the realizability constraint is active even in this case, as we can see in figures 4.2 and 4.3 showing mean velocity profiles and skin friction coefficients. The realizability constraint exploits the symmetry of the strain rate tensor, and changes the coordinate system to the principal one, effectively transforming the original flow to that of a pure strain - in which the strain rate tensor is diagonal. An upper bound on the time scale is imposed by constraining the diagonal components of the strain rate (corresponding to the eigenvalues), but the bound was derived in principal axes and not the original coordinate system. Therefore the realizability constraint can be active in general flow configurations because it only matters whether the magnitude of the strain rate is high enough so that the fraction proportional to $1/\varphi|S|$ is smaller than k/ε.

The application of the realizability constraint on Reynolds stress or eddy viscosity results in overprediction of the recirculation length (see table A.3 and also figure 4.3 a)), but the predicted separation point is closer to the point predicted by the DNS than the one obtained by the plain $\varphi - f$ model. Since the recirculation length is overpredicted, the mean velocity profiles sampled at Station 1 (figure 4.2 a)) are in a worse agreement with the DNS data than the $\varphi - f$ model without realizability constraints. The first peak in skin friction coefficient distribution along the inner wall (somewhere around Station 2) and the second peak along the outer wall (somewhere around Station 3) are even more overpredicted when the realizability constraints are applied, which is counterintuitive. We should also remind ourselves that no curvature corrections were used and the effect of streamline curvature is present, but never accounted for, so the overly comprehensive assessment of the results is out of place. But overall, the result of applying the stress or viscosity limiter is not that disruptive.

Note that limiting the production to dissipation ratio $\mathcal{P}_k/\varepsilon$ is necessary in

the context of some curvature correction proposals. Cazalbou [43] designed a curvature correction of the $k-\varepsilon$ model based on sensitizing the $C_{\varepsilon 2}$ coefficient to both rotation and curvature. The precise formula for the sensitized coefficient is not important, it's only crucial to realize that it linearly depends on the ratio $\sqrt{2}|S|k/\varepsilon$. The $k-\varepsilon$ model can predict unrealistically high values of the ratio $\sqrt{2}|S|k/\varepsilon$ in general 3D computations, which will result in excessively high values of the sensitized coefficient $C_{\varepsilon 2}$. The authors of the article [44] suggested two solutions to this problem. We can either limit the coefficient directly or limit the production rate $\mathcal{P}_k$. Because the ratio $\sqrt{2}|S|k/\varepsilon$ is proportional to the square root of the production-to-dissipation ratio, it's apparent how applying the realizability constraint to the production rate would be helpful to bound the sensitized coefficient to a reasonable range of values.

Let's address the effects of applying the time-scale limiter to the $\varphi - f$ model on the results. Note that what the author calls a time-scale limiter is a realizability constraint applied to the eddy viscosity (therefore also bounding the production rate) plus dividing the source terms of the ε equation by the bounded time scale. The enhancement of dissipation rates resulting from amplifying the term $C_{\varepsilon 1}\mathcal{P}_k - C_{\varepsilon 2}\varepsilon$ is undesirable in this case. The predicted recirculation length by the $\varphi - f$ model with the time-scale limiter is more than twice higher than the one predicted by the DNS. Notice also that the predicted mean velocity profiles sampled at all four stations are clearly at odds with the DNS data. We shall analyze the modified source term in the ε equation to see how it changes both k and ε equations.

The discussion will be constrained to the 3D variant of the realizability constraint and $\varphi - f$ model, the results will be analogous to the 2D variant of the realizability constraint and can be derived even for the $k-\varepsilon$ model. The superscript lim will denote bounded quantities, no superscript will mean standard definitions for the time scale and production rate, $T = k/\varepsilon$ and $\mathcal{P}_k = 2\nu_T|S|^2$. Let us again state the bounded time scale for the reader's convenience:

$$T^{lim} = \frac{C_{lim}}{\sqrt{3}\varphi C_\mu \sqrt{2|S|^2}}, \tag{4.2}$$

and also the bounded production rate:

$$\mathcal{P}_k^{lim} = C_{lim}\frac{k}{\sqrt{3}}\sqrt{2|S|^2}. \tag{4.3}$$

Now substituting the linearized production (4.3) and the bounded time scale (4.2) to the expression $(C_{\varepsilon 1}\mathcal{P}_k - C_{\varepsilon 2}\varepsilon)/T$ yields:

$$\begin{aligned}\frac{C_{\varepsilon 1}\mathcal{P}_k^{lim} - C_{\varepsilon 2}\varepsilon}{T^{lim}} &= C_{\varepsilon 1}C_\mu k\varphi 2|S|^2 - \frac{C_{\varepsilon 2}\varphi\sqrt{3}\sqrt{2|S|^2}}{C_{lim}}\varepsilon \\ &= C_{\varepsilon 1}\frac{\mathcal{P}_k}{T} - C_{\varepsilon 2}\frac{\varepsilon}{T^{lim}}.\end{aligned}$$

We have recovered the standard source term $C_{\varepsilon 1}\mathcal{P}_k/T$ without realizability constraints and an amplified sink $C_{\varepsilon 2}\varepsilon/T^{lim}$. So why are the dissipation rates so grossly overestimated? We must not forget the k equation, where the right-hand side is exactly $\mathcal{P}_k - \varepsilon$. In the regions where the time scale limiter is active, the source term of the k equation is linearized production rate $\mathcal{P}_k^{lim}$ but the production rate appearing in the ε equation is quadratic in the strain rate magnitude, thus we have mismatched sources in the two equations, their ratio is proportional to $\mathcal{P}_k/\mathcal{P}_k^{lim} \propto T/T^{lim}$. Well, it's obvious if one writes it down, but still, this is a drastic alteration of this pair of equations, inconsistent with the original $k-\varepsilon$ model. An immediate difficulty related to the curvature corrections arises. Even if we derived a curvature correction for the $\varphi - f$ model by sensitizing the $C_{\varepsilon 2}$ coefficient in hopes of improved predictions, the effect of the curvature correction could get dominated by the altered set equations if the time-scale limiter was applied in conjunction.

4.3 Issues with implementation of stress limiters in $k-\omega$ models

It was already stated in the earlier chapters that Wilcox's $k-\omega$ model from 2006 and the updated version of the $k-\omega$ SST model from 2003 embed some stress limiter in their formulations. It wasn't strictly necessary to discuss the precise formulation of these two models, but after the terrible revelation in the previous section, we should be more cautious than ever.

The k equation for both models is the same and analogous to the $k-\varepsilon$ models:

$$\frac{\mathrm{D}k}{\mathrm{D}t} = \mathcal{P}_k - \beta^*\omega k + \frac{\partial}{\partial x_j}\left[\left(\nu + \sigma_k \frac{k}{\omega}\right)\frac{\partial k}{\partial x_j}\right]. \tag{4.4}$$

Note that the fraction k/ω has the same dimensions as eddy viscosity. Wilcox formulated the equation for ω as the following:

$$\frac{\mathrm{D}\omega}{\mathrm{D}t} = \frac{\gamma\omega}{k}\mathcal{P}_k - \beta\omega^2 + \frac{\partial}{\partial x_j}\left[\left(\nu + \sigma_\omega \frac{k}{\omega}\right)\frac{\partial \omega}{\partial x_j}\right] + \frac{\sigma_d}{\omega}\frac{\partial k}{\partial x_j}\frac{\omega}{\partial x_j}. \tag{4.5}$$

We haven't yet encountered a definition of eddy viscosity, which in this formulation is present only in the closure of the Reynolds stress tensor and its possible limiting will only alter the production rate in this pair of equations. So here it is:

$$\nu_T = \frac{k}{\hat{\omega}}; \quad \hat{\omega} = \max\left\{\omega, C_{lim}\sqrt{\frac{2|S|^2}{\beta^*}}\right\}; \tag{4.6}$$

and the limiter imposed on ω is essentially a realizability constraint, albeit with different constants, because the upper bound for ω derived the same way as Durbin's upper bound for the time scale reads:

$$\omega \leq \sqrt{3}C_{lim}\sqrt{2|S|^2}. \tag{4.7}$$

If the limiter written in equation (4.6) is active, the production rate is again linearized (denoted $\hat{\mathcal{P}}_k$):

$$\hat{\mathcal{P}}_k = \frac{\sqrt{\beta^*}}{C_{\text{lim}}} k \sqrt{2|S|^2}, \tag{4.8}$$

note that the pedantic distinction between k/ω and $\nu_T = k/\hat{\omega}$ is crucial because the source term in ω equation involving the production rate $\hat{\mathcal{P}}_k$ is linear in the strain rate magnitude, thus consistent with the production rate in the k equation:

$$\begin{aligned} \gamma \frac{\omega}{k} \hat{\mathcal{P}}_k &= \gamma \frac{\omega}{k} \frac{k}{\hat{\omega}} 2|S|^2 \\ &= \gamma \omega \frac{\sqrt{\beta^*}}{C^{lim}} \sqrt{2|S|^2}. \end{aligned}$$

Unfortunately, this is not how the model that the author used for the impinging jet case was implemented. The stark difference between the used implementation and the official formulation boils down to the abuse of notation, all the fractions k/ω were reinterpreted as the eddy viscosity. Suppose that the limiter on ω (4.6) is active, the production rate in the k equation is linearized in the strain rate magnitude, but the source term in the ω equation has now the form:

$$\gamma \frac{\mathcal{P}_k}{\nu_T} = \gamma 2|S|^2, \tag{4.9}$$

as if no limiter on ω was applied and the inconsistency issue regarding different production rates in both k and ω is analogous to the issue with the time scale limiter applied on the $\varphi - f$ model. The effects of this alteration can be again seen in figures 4.2, 4.3 (and in table 4.1) where also predictions by the original formulation with and without the stress limiter are plotted. A familiar situation arises: the predictions are the best when no limiter is applied, and the stress limiter alters the velocity profiles and skin friction coefficient only slightly. Only when the production rates are different in each equation and ω is overproduced are the results at serious odds with the data. It has to be remarked that the separation length is overpredicted even without a stress limiter, but the separation point is the closest to the one predicted by the DNS.

Equations for k, ω are very similar in $k-\omega$ SST model, except that the coefficients $\gamma, \beta, \sigma_k, \sigma_\omega$ are blends of inner (1) and outer (2) constants and the cross-diffusion term is faded out outside the boundary layer. The first notable difference from Wilcox's model relevant to the current discourse is that the fraction k/ω is always interpreted as eddy viscosity, so the source term in the ω equation is $\mathcal{P}_k \gamma / \nu_T$. The model uses a viscosity limiter that reads:

$$\nu_T = \frac{a_1 k}{\max\left\{a_1 \omega, \sqrt{2|S|^2} F_2\right\}}. \tag{4.10}$$

The presence of a blending function F_2 indicates that the limiter can be active only in the near wall regions, far away from the walls the formula (4.10) will always collapse to the fraction k/ω. The model also employs a simple production limiter:

$$\tilde{\mathcal{P}_k} = \max\{\mathcal{P}_k, 10\beta^* k\omega\}, \tag{4.11}$$

which ensures that the production rate never exceeds the dissipation rate by a factor of 10. Now suppose that the viscosity limiter is active in the boundary layer so that the eddy viscosity is bounded:

$$\nu_T \leq \frac{a_1 k}{\sqrt{2|S|^2}}, \tag{4.12}$$

the production rate is again bounded by an expression linear in the strain rate magnitude: $\mathcal{P}_k \leq a_1 k\sqrt{2|S|^2}$. Unfortunately, in the source term in the ω, the linearized production rate will be canceled by limited eddy viscosity, resulting again in $\mathcal{P}_k\gamma/\nu_T = \gamma 2|S|^2$. Perhaps even more bizarre is to consider a combination where a viscosity limiter is active, but the production rate is also bounded by $10\beta^* k\omega$ (formula (4.11)). Then the source term in ω equation reads:

$$\begin{aligned}\gamma\frac{\tilde{\mathcal{P}}_k}{\nu_T} &\leq \gamma\frac{10\beta^* k\omega}{a_1 k}\sqrt{2|S|^2} \\ &\leq \gamma\frac{10}{a_1}\beta^*\omega\sqrt{2|S|^2},\end{aligned}$$

and production rate in the k equation is bounded by $10\beta^* k\omega$. There is no correspondence between the production rates in k and ω equations. Note that the $k-\omega$ SST model was intentionally formulated like this. Again, these alterations are significant in the context of curvature/rotation corrections. In the formulation of a particular correction for the $k-\omega$ SST model [45], authors clearly specify that the "base" model should be the original one, which uses a different eddy viscosity limiter. If one chooses to implement this correction into the 2003 version instead, omitting the difference in the eddy viscosity limiters, one could potentially obtain vastly different results. These substitutions demonstrate that even a slight reinterpretation of the original formulations of $\varphi-f$ and $k-\omega$ models can lead to profoundly different sets of scale-determining equations, ones which grossly overproduce the dissipation rates, once the corresponding limiters are active.

A little side note on the predictions of separation points: it is a widely known fact (was also discussed in subsection 3.4.3) that $k-\varepsilon$ models tend to overproduce turbulence kinetic energy in case of adverse pressure gradient layers, therefore predicting flows with pressure-induced separation which stay attached further than they should be. On the other hand, $k-\omega$ models provide better predictions, while tending to undershoot the separation point. We can see this in figure 4.3 (or more clearly in table 4.1), the $\varphi-f$ model (no limiters)

overshoots the separation point because it still relies on the $k-\varepsilon$ to determine the time scale and kinetic energy. Wilcox's $k-\omega$ (no limiters) undershoots it but is in almost perfect agreement with the DNS. But when the production rates are limited, the $\varphi - f$ model undershoots the separation point. So is the tendency of $k-\varepsilon$ models to predict flows that stay attached further than they should be purely caused by the ε equation (Wilcox argues that the ε equation misses cross-diffusion) or is it again a problem of the formula $2\nu_T|S|^2$ overpredicting the production rates? A strong adverse pressure gradient also means large deceleration. Perhaps we are in a situation similar to stagnation anomaly, although not as extreme.

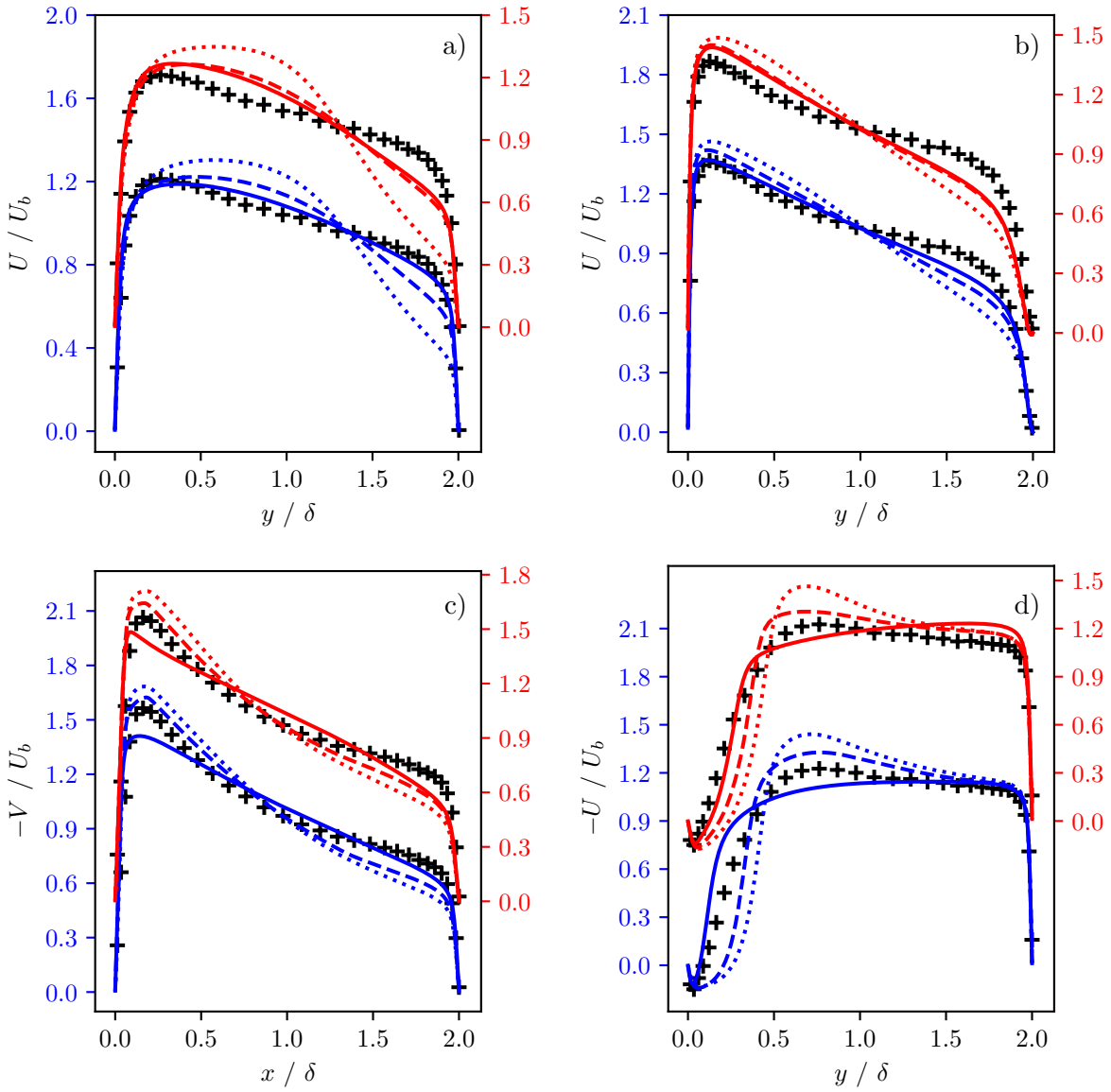

Figure 4.2: Computed profiles of mean velocity. Profiles are shifted for clarity, and the axes for shifted and non-shifted profiles are distinguished by color. a) Station 1; b) Station 2; c) Station 3; d) Station 4; —— $\varphi - f$ without modifications, - - - - $\varphi - f$ with stress limiter; ····· $\varphi - f$ with time-scale limiter; —— $\varphi - f$ with time-scale limiter; —— $k-\omega$ without a stress limiter; - - - - $k-\omega$ with a stress limiter; ····· $k-\omega$ implemented inconsistently; + DNS data [7].

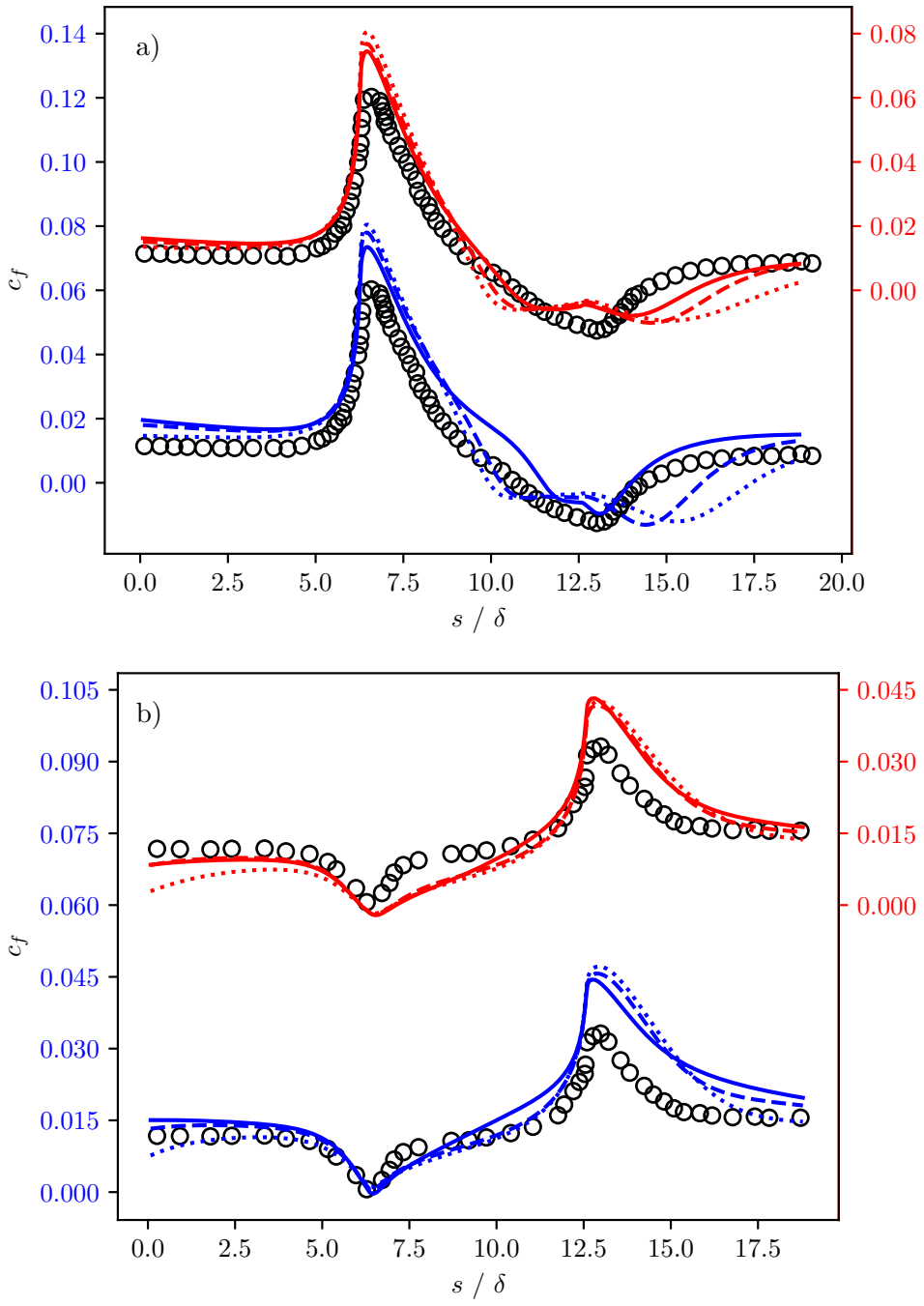

Figure 4.3: Computed skin friction coefficients along the inner and outer wall of the upper U-bend (Station 1-4). a) inner wall; b) outer wall; Legend is provided in a caption of the figure 4.2.

Conclusion

A particular turbulence model augmented with elliptic relaxation was chosen as a basis for subsequent computations. The author hopes that the elliptic relaxation concept was given enough exposition to convince the reader, that capturing high anisotropy of turbulence in the vicinity of walls is a crucial factor for correct modeling of turbulent transport to/from the walls. Elliptic relaxation is a framework since it isn't necessarily bound to a $k-\varepsilon$ model.

The model, designated as $\varphi - f$, is still based on the eddy viscosity concept and inevitably suffers from the deficiencies of the Boussinesq hypothesis. Eddy viscosity models tend to overproduce turbulence kinetic energy in flows involving stagnation regions. The stagnation anomalies are certainly linked to the formula for the production rate of kinetic energy $2\nu_T|S|^2$ closed with eddy viscosity assumption. Possible remedies were introduced to suppress the problem. But there is one that the author likes in particular - a realizability constraint. A realizability constraint bounds the normal Reynolds stresses to their physically permissible range. Although Durbin formulated this constraint only after it was obvious that stagnation anomalies are a problem, which has to be dealt with. What's so attractive about such a constraint, is that it is in a sense a priori. One doesn't need any prior knowledge about any eddy viscosity model or experience with using such models to conclude that bounding normal stresses is very reasonable. This is certainly not the case with other modifications: Kato-Launder modification exploits the fact once the fluid starts rapidly accelerating in the direction of the streamlines, the magnitude of the symmetric velocity gradient will be much higher than that of vorticity, hence the modification of production rate is simply $2\nu_T|S||\Omega|$. The author's modifications are based on a similar idea, they all enhance dissipation rates in proportion to the fluid's acceleration in the direction of the streamlines. The Yap correction is often misused as a remedy for stagnation anomalies, but at least it was found that the overproduction of kinetic energy can be compensated with increased near-wall dissipation rates without necessarily targeting the true cause of the problem.

It is perhaps an understatement to say that details about the derivation and implementation of the realizability constraint are tricky. Stemming from the way how the realizability constraint was derived, it ultimately depends only on the magnitude of the symmetric velocity gradient to be high enough to overcome the turbulence quantity we are trying to constrain to trigger the limiter. This results in uncertainty, we can't possibly predict where the corresponding limiter will be active and how substantial the change of predictions is going to be. In the impinging jet case, it is obvious that the limiter should be active and the results were improved accordingly. But in the infinite serpentine, the situation is more problematic. The application of the stress limiter was strictly unnecessary in case of the Wilcox's $k-\omega$ model, but the $\varphi-f$ model could benefit from at least some production rate limiting to drive the separation point closer to the DNS data, but the stress limiter was either too strong or was active even in the recirculation region, resulting in overpredicted recirculation length. Unfortunately, the strength of the limiter can be only modulated by changing the corresponding multiplicative constant. What is also clear from the predictions of the mean velocity profiles and recirculation lengths in the infinite serpentine is that the eddy viscosity models are perfectly capable of predicting mean flow quantities in a reasonable agreement with the data, even when the magnitude of symmetric velocity gradient is sufficiently high to throw the normal stresses out of their permissible range. We have found ourselves in the most unfortunate situation, a fix of one problem introduces other problems. The realizability constraint is the only modification that can be naturally included in the formulation of any eddy viscosity model. It is hard to tell whether it is generally appropriate to use it, sometimes it solves problems, and other times it becomes the problem.

The situation gets even more difficult, that the realizability constraint can be implemented in multiple ways and the discrepancy can be vast. It can be implemented as a stress limiter, where strictly only the Reynolds stress is bounded, resulting in linearized production rates in the equation for k and an equation for the second variable. One can also interpret the realizability constraint as an eddy viscosity limiter, hence we have to bound every instance of ν_T appearing in the equations. It was found that these two limiters produce essentially the same results. Substantial change comes when one interprets the derived bound on either the turbulence time scale T or ω as a literal bound, thus applying the limiter on every instance of T, ω. This slight change in notation results in a complete alteration of the pair of corresponding scale-determining equations once such a limiter is active. The production rates in both equations don't correspond to each other, the production rate in the k equation is linear in the magnitude of symmetric velocity gradient while the source term in the equation for the second variable is quadratic. Under such conditions, the production rates get overcompensated by the dissipation rates. First of all, it's trivial to observe that such alterations are favorable for flows experiencing stagnation. If we look again at the figure 3.6 comparing the stress

and time-scale limiter in the case of the $\varphi - f$ model, the time-scale limiter is a better option. But why do as much as to completely alter the model to arrive at a better result? There are perhaps two reasons for that. After a stress limiter is applied, the production rates are now linear in the symmetric velocity gradient magnitude, but this can still be qualitatively wrong, since increasing components of the symmetric gradient will always increase $\mathcal{P}_k \propto k|S|$, because the formula for the production rates can only possibly permit an increase. Note that the production rate of kinetic energy should be just half of the trace of the production tensor thus it can freely increase or decrease irrespective of the magnitude of the symmetric gradient. With a time-scale limiter, we can compensate for this deficit. The second reason is probably compensation for unknown sources of dissipation, which are not included in the ε equation. Nevertheless, it is certainly useful, an analogous thing was done in the formulation of the 2003 $k - \omega$ SST model, primarily designed for aeronautical applications - it's obvious that for these flow configurations, suppressing the overproduction of kinetic energy in the stagnation regions is so important, that one has to resort to such alterations. But the realizability constraint is volatile and can switch on even when it isn't appropriate - once the production rates in the two equations don't correspond to each other when they perhaps should have been left alone, a catastrophe is upon us. We have seen this, in the infinite serpentine, the overprediction of recirculation length caused by the stress limiter was tolerable, but the time scale limiter caused the predicted recirculation length to be at least two times higher than the result obtained from the DNS, which ultimately led to poorly predicted mean velocity profiles. So what should we generally use? Perhaps one should swallow the bitter pill and go with the plain stress limiter - it doesn't work as well as the time scale limiter in suppressing stagnation anomalies, but at least won't spoil the results too much in case it is not appropriate to use. Or maybe we should stick to the time scale limiter, but adjust the multiplicative constant C_{lim} case by case...and that would be overfitting.

Overfitting is generally frowned upon in any scientific community, however, the author senses its insidious prevalence in the general use of eddy viscosity models, and the line between overfitting and just plain fitting is blurred. For instance: we start with a flow configuration where a stress limiter is necessary, then we want to apply the same model to some flow in a rotating frame of reference. Hence the model would benefit from a rotation correction and the stress limiter should be switched off since rotation/curvature corrections are more often than not, derived from the analysis of homogenous turbulence, and the limiter could interfere with the calibration. Although there is no explicit overfitting involved, we have preemptively changed the model to better fit the data. This is not that different from changing the values of free coefficients corresponding to some modification in hopes of improving the agreement with the data, although not as explicit in its ad hocness. Models using the eddy viscosity concept are so fundamentally broken, that very good agreement with

the validation data can be obtained only with some ad hoc explicit specialization of the model if the various cases considered are vastly different. Models seem to be more like templates ready for specific applications. It doesn't matter if one fiddles with the coefficients to arrive at a better result or if one decides to use a more "appropriate" formulation of the model for the case at hand. The underlying problem isn't the actual fine-tuning itself, but the flow configurations upon which it is based - the configurations are sufficiently simple that there are only one or two dominant features for which the model has to be adjusted. In the impinging jet case, it was the inviscid stagnation, and in infinite serpentine, it was streamline curvature and pressure-induced separation. But we haven't considered a possible configuration, where all three of these features are present. Then we are again stuck with such a modification, that doesn't work too well for one problem and doesn't spoil the results too much if it is not appropriate to use - a stress limiter.

It seems to the author that the only way to properly get out of this dilemma is to reject the Boussinesq altogether and use full second-moment closures instead. None of the issues discussed above ever apply to Reynolds stress models, there is no stagnation anomaly or insensitivity to curvature/rotation. The concept of a "remedy" or a "correction" doesn't make sense in full second-moment closures. The author will try his best to gain more insight into the principles of Reynolds stress modeling.

Bibliography

[1] Moser, R. D.; Kim, J.; et al. Direct numerical simulation of turbulent channel flow up to Re=590. *Physics of Fluids*, volume 11, no. 4, 04 1999: pp. 943–945, ISSN 1070-6631, doi: 10.1063/1.869966, https://pubs.aip.org/aip/pof/article-pdf/11/4/943/12607456/943_1_online.pdf. Available from: https://doi.org/10.1063/1.869966

[2] Baughn, J. W.; Shimizu, S. Heat Transfer Measurements From a Surface With Uniform Heat Flux and an Impinging Jet. *Journal of Heat Transfer*, volume 111, no. 4, 11 1989: pp. 1096–1098, ISSN 0022-1481, doi:10.1115/1.3250776, https://asmedigitalcollection.asme.org/heattransfer/article-pdf/111/4/1096/5910138/1096_1.pdf. Available from: https://doi.org/10.1115/1.3250776

[3] Cooper, D.; Jackson, D.; et al. Impinging jet studies for turbulence model assessment—I. Flow-field experiments. *International Journal of Heat and Mass Transfer*, volume 36, no. 10, 1993: pp. 2675–2684, ISSN 0017-9310, doi:https://doi.org/10.1016/S0017-9310(05)80204-2. Available from: https://www.sciencedirect.com/science/article/pii/S0017931005802042

[4] Baughn, J. W.; Hechanova, A. E.; et al. An Experimental Study of Entrainment Effects on the Heat Transfer From a Flat Surface to a Heated Circular Impinging Jet. *Journal of Heat Transfer*, volume 113, no. 4, 11 1991: pp. 1023–1025, ISSN 0022-1481, doi: 10.1115/1.2911197, https://asmedigitalcollection.asme.org/heattransfer/article-pdf/113/4/1023/5910269/1023_1.pdf. Available from: https://doi.org/10.1115/1.2911197

[5] Jungho Lee, S.-J. L. Stagnation region heat transfer of a turbulent axisymmetric het impingement. *Experimental Heat Transfer*, volume 12, no. 2, 1999: pp. 137–156, doi:10.1080/089161599269753, https://

doi.org/10.1080/089161599269753. Available from: https://doi.org/10.1080/089161599269753

[6] Schlatter, P.; Örlü, R. Assessment of direct numerical simulation data of turbulent boundary layers. *Journal of Fluid Mechanics*, volume 659, 2010: p. 116–126, doi:10.1017/S0022112010003113.

[7] Laskowski, G. M.; Durbin, P. A. Direct numerical simulations of turbulent flow through a stationary and rotating infinite serpentine passage. *Physics of Fluids*, volume 19, no. 1, 01 2007, ISSN 1070-6631, doi:10.1063/1.2404940, 015101, https://pubs.aip.org/aip/pof/article-pdf/doi/10.1063/1.2404940/15771361/015101_1_online.pdf. Available from: https://doi.org/10.1063/1.2404940

[8] Durbin, P.; Reif, B. Statistical Theory and Modeling for Turbulent Flows, Second Edition, Second Edition. *Statistical Theory and Modeling for Turbulent Flows: Second Edition*, 01 2011, doi:10.1002/9780470972076.

[9] Durbin, P. A. Near-wall turbulence closure modeling without "damping functions". *Theoretical and Computational Fluid Dynamics*, volume 3, 1991: pp. 1–13.

[10] Daly, B. J.; Harlow, F. H. Transport Equations in Turbulence. *The Physics of Fluids*, volume 13, no. 11, 11 1970: pp. 2634–2649, ISSN 0031-9171, doi:10.1063/1.1692845, https://pubs.aip.org/aip/pfl/article-pdf/13/11/2634/12626086/2634_1_online.pdf. Available from: https://doi.org/10.1063/1.1692845

[11] Rotta, J. Statistical theory of nonhomogenous turbulence. II. *Z. Physik*, volume Vol: 131, 1 1951, doi:10.1007/BF01329645. Available from: https://www.osti.gov/biblio/4391207

[12] Launder, B. E.; Shima, N. Second-moment closure for the near-wall sublayer - Development and application. *AIAA Journal*, volume 27, no. 10, 1989: pp. 1319–1325, doi:10.2514/3.10267, https://doi.org/10.2514/3.10267. Available from: https://doi.org/10.2514/3.10267

[13] Manceau, R.; Hanjalic, K. Elliptic blending model: A new near-wall Reynolds-stress turbulence closure. *Physics of Fluids, 14 (2), 2002 ; doi:10.1063/1.1432693*, volume 14, 02 2002, doi:10.1063/1.1432693.

[14] Manceau, R.; Wang, M.; et al. Inhomogeneity and anisotropy effects on the redistribution term in Reynolds-averaged Navier–Stokes modelling. *Journal of Fluid Mechanics*, volume 438, 2001: p. 307–338, doi:10.1017/S0022112001004451.

[15] Hanjalić, K.; Popovac, M.; et al. A robust near-wall elliptic-relaxation eddy-viscosity turbulence model for CFD. *International Journal of Heat and Fluid Flow*, volume 25, no. 6, 2004: pp. 1047–1051, ISSN 0142-727X, doi:https://doi.org/10.1016/j.ijheatfluidflow.2004.07.005. Available from: `https://www.sciencedirect.com/science/article/pii/S0142727X0400116X`

[16] Lien, F.-S.; Kalitzin, G. Computations of transonic flow with the v2–f turbulence model. *International Journal of Heat and Fluid Flow*, volume 22, 02 2001: pp. 53–61, doi:10.1016/S0142-727X(00)00073-4.

[17] Laurence, D.; Uribe, J.; et al. A robust formulation of the v2f model. *Flow, Turbulence and Combustion*, volume 73, 03 2005: pp. 169–185, doi:10.1007/s10494-005-1974-8.

[18] Davidson, L.; Nielsen, P.; et al. Modifications of the V2 Model for Computing the Flow in a 3D Wall Jet. In *Proceedings of the International Symposium on Turbulence, Heat and Mass Transfer, October 12 - 17, 2003, Antalya, Turkey.*, 2003, iSSN ; - ; Modifications of the Model for Computing the Flow in a 3D Wall Jet ; Conference date: 19-05-2010.

[19] Manceau, R.; Carlson, J. R.; et al. A rescaled elliptic relaxation approach: Neutralizing the effect on the log layer. *Physics of Fluids*, volume 14, no. 11, 09 2002: pp. 3868–3879, ISSN 1070-6631, doi:10.1063/1.1511547. Available from: `https://doi.org/10.1063/1.1511547`

[20] Lee, J.; Lee, S.-J. The effect of nozzle configuration on stagnation region heat transfer enhancement of axisymmetric jet impingement. *International Journal of Heat and Mass Transfer - INT J HEAT MASS TRANSFER*, volume 43, 09 2000: pp. 3497–3509, doi:10.1016/S0017-9310(99)00349-X.

[21] Moukalled, F.; Mangani, L.; et al. *The Finite Volume Method in Computational Fluid Dynamics: An Advanced Introduction with OpenFOAM® and Matlab®*, volume 113. 10 2015, ISBN 978-3-319-16873-9, doi:10.1007/978-3-319-16874-6.

[22] Zuckerman, N.; Lior, N. Radial Slot Jet Impingement Flow and Heat Transfer on a Cylindrical Target. *Journal of Thermophysics and Heat Transfer - J THERMOPHYS HEAT TRANSFER*, volume 21, 07 2007: pp. 548–561, doi:10.2514/1.20829.

[23] ANSYS. Best Practice RANS Turbulence Modeling in Ansys CFD. `https://www.ansys.com/resource-center/technical-paper/best-practice-rans-turbulence-modeling-in-ansys-cfd`, Mar. 2022.

[24] Wilcox, D. C. *Turbulence modeling for CFD / by David C. Wilcox.* La Cañada, Calif.: DCW Industries, third edition, 2006, ISBN 9781928729082.

[25] Kato, M.; Launder, B. The Modelling of Turbulent Flow Around Stationary and Vibrating Square Cylinders. 01 1993.

[26] Durbin, P. On the k-3 stagnation point anomaly. *International Journal of Heat and Fluid Flow*, volume 17, no. 1, 1996: pp. 89–90, ISSN 0142-727X, doi:https://doi.org/10.1016/0142-727X(95)00073-Y. Available from: `https://www.sciencedirect.com/science/article/pii/0142727X9500073Y`

[27] Sveningsson, A.; Davidson, L. Assessment of realizability constraints in turbulence models. *International Journal of Heat and Fluid Flow*, volume 25, 10 2004: pp. 785–794, doi:10.1016/j.ijheatfluidflow.2004.05.014.

[28] Yap, C. R. *Turbulent heat and momentum transfer in recirculating and impinging flows*. Dissertation thesis, University of Manchester, UK, Jan. 1987.

[29] Development and application of a cubic eddy-viscosity model of turbulence. *International Journal of Heat and Fluid Flow*, volume 17, no. 2, 1996: pp. 108–115, ISSN 0142-727X, doi:https://doi.org/10.1016/0142-727X(95)00079-6. Available from: `https://www.sciencedirect.com/science/article/pii/0142727X95000796`

[30] Salamah, S. A.; Kaminski, D. A. Modeling of Turbulent Heat Transfer from an Array of Submerged Jets Impinging on a Solid Surface. *Numerical Heat Transfer, Part A: Applications*, volume 48, no. 4, 2005: pp. 315–337, doi:10.1080/10407780590945551, `https://doi.org/10.1080/10407780590945551`. Available from: `https://doi.org/10.1080/10407780590945551`

[31] Ahmadi, H.; Rajabi Zargarabadi, M.; et al. Numerical modeling of a turbulent semi-confined slot jet impinging on a concave surface. *Thermal Science*, volume 19, 01 2013: pp. 57–57, doi:10.2298/TSCI121003057A.

[32] Launder, B.; Sharma, B. Application of the energy-dissipation model of turbulence to the calculation of flow near a spinning disc. *Letters in Heat and Mass Transfer*, volume 1, no. 2, 1974: pp. 131–137, ISSN 0094-4548, doi:https://doi.org/10.1016/0094-4548(74)90150-7. Available from: `https://www.sciencedirect.com/science/article/pii/0094454874901507`

[33] Wang, S.; Mujumdar, A. A comparative study of five low Reynolds number k– models for impingement heat transfer. *Applied Thermal Engineering*, volume 25, no. 1, 2005: pp. 31–44, ISSN 1359-4311, doi:https:

//doi.org/10.1016/j.applthermaleng.2004.06.001. Available from: https://www.sciencedirect.com/science/article/pii/S1359431104001413

[34] Hanjalic´, K.; Launder, B. E. Sensitizing the Dissipation Equation to Irrotational Strains. *Journal of Fluids Engineering*, volume 102, no. 1, 03 1980: pp. 34–40, ISSN 0098-2202, doi:10.1115/1.3240621, https://asmedigitalcollection.asme.org/fluidsengineering/article-pdf/102/1/34/5898486/34_1.pdf. Available from: https://doi.org/10.1115/1.3240621

[35] Tennekes, H.; Lumley, J. L. A First Course in Turbulence. Jan 1972, doi:10.7551/mitpress/3014.001.0001.

[36] Yoshizawa, A. Statistical modeling of a transport equation for the kinetic energy dissipation rate. *The Physics of Fluids*, volume 30, no. 3, 03 1987: pp. 628–631, ISSN 0031-9171, doi:10.1063/1.866366, https://pubs.aip.org/aip/pfl/article-pdf/30/3/628/12611272/628_1_online.pdf. Available from: https://doi.org/10.1063/1.866366

[37] Bredberg, J. On Two-Equation Eddy-Viscosity Models. Technical report 01/8, Department of Thermo and Fluid Dynamics, Chalmers University of Technology, Gothenburg, Sweden, 2001.

[38] Hanjalic, K.; Launder, B. E. Turbulent Transport Modelling of Separating and Reattaching Shear Flows - 1. Basic Multi-Scale Development and Its Application to Thin Shear Flows. Mechanical Engineering Report TF/78/9, University of California, Davis, Davis, CA, USA, 1978.

[39] Hellsten, A.; Bézard, H. Behaviour of Nonlinear Two-Equation Turbulence Models at the Free-Stream Edges of Turbulent Flows. In *Engineering Turbulence Modelling and Experiments 6*, edited by W. Rodi; M. Mulas, Amsterdam: Elsevier Science B.V., 2005, ISBN 978-0-08-044544-1, pp. 147–156, doi:https://doi.org/10.1016/B978-008044544-1/50013-3. Available from: https://www.sciencedirect.com/science/article/pii/B9780080445441500133

[40] Hellsten, A. *New two-equation turbulence model for aerodynamics applications*. Doctoral thesis, 2004.

[41] Menter, F.; Kuntz, M.; et al. Ten years of industrial experience with the SST turbulence model. *Heat and Mass Transfer*, volume 4, 01 2003.

[42] Menter, F.; Smirnov, P.; et al. A One-Equation Local Correlation-Based Transition Model. *Flow, Turbulence and Combustion*, volume 95, 07 2015: pp. 1–37, doi:10.1007/s10494-015-9622-4.

[43] Cazalbou, J.-B.; Chassaing, P.; et al. Two-equation modeling of turbulent rotating flows. *Physics of Fluids*, volume 17, no. 5, 05 2005, ISSN 1070-6631, doi:10.1063/1.1920630, 055110, https://pubs.aip.org/aip/pof/article-pdf/doi/10.1063/1.1920630/14772473/055110_1_online.pdf. Available from: https://doi.org/10.1063/1.1920630

[44] Dufour, G.; Cazalbou, J.-B.; et al. Assessing Rotation/Curvature Corrections to Eddy-Viscosity Models in the Calculations of Centrifugal-Compressor Flows. *Journal of Fluids Engineering*, volume 1, 09 2008: pp. pp. 091401–091411, doi:10.1115/1.2953231.

[45] Smirnov, P.; Menter, F. Sensitization of the SST Turbulence Model to Rotation and Curvature by Applying the Spalart–Shur Correction Term. *Journal of Turbomachinery-transactions of The Asme - J TURBOMACH-T ASME*, volume 131, 10 2009, doi:10.1115/1.3070573.

[46] Roache, P. J. Perspective: A Method for Uniform Reporting of Grid Refinement Studies. *Journal of Fluids Engineering*, volume 116, no. 3, 09 1994: pp. 405–413, ISSN 0098-2202, doi:10.1115/1.2910291, https://asmedigitalcollection.asme.org/fluidsengineering/article-pdf/116/3/405/5531128/405_1.pdf. Available from: https://doi.org/10.1115/1.2910291

Appendix **A**

Grid refinement studies

Grid refinement studies were done for all the cases considered in this thesis. The report of the studies will be done in accordance with the method first introduced by Roache [46], which is based on Richardson's extrapolation. First some suitable quantity of interest f has to be defined, with which the whole convergence study will be conducted. All studies were done over three grids, with **constant refinement ratio** $\mathbf{r} \doteq \sqrt{\mathbf{2}}$, order of convergence was thus established as the following:

$$p = \ln\left(\frac{f_3 - f_2}{f_2 - f_1}\right) / \ln(r).$$

The grids and quantities f are indexed from finest to coarsest mesh in ascending order, so "Grid 1" will denote the finest grid, and f_1 is the quantity of interest obtained from the finest grid. Since three grids were considered, the factor of safety could be set to $F_a = 1.25$ in the definition of grid convergence index:

$$GCI = \frac{F_a|\varepsilon|}{(r^p - 1)},$$

where the relative error $\varepsilon = (f_2 - f_1)/f_1$. The most important aspect of these convergence studies is to find out whether the solutions lie within the asymptotic range of convergence, in other words, the following ratio has to be close to unity:

$$C = r^p \frac{GCI_{12}}{GCI_{23}} \approx 1.$$

A.1 Impinging jet, cases $H/D = 2$, $H/D = 6$

We were primarily focused on correctly predicting the heat transfer rates for both cases, so a surface averaged temperature flux from the plate $\overline{\dot{q}}$ was defined

to quantify discrepancies between the three grids:

$$\overline{\dot{q}} = \frac{\iint_{r \le r_{lim}} \nabla \mathbf{T} \cdot \mathrm{d}\mathbf{S}}{\iint_{r \le r_{lim}} 1 \mathrm{d}S}.$$

The value of $r_{lim} = 3.5D$ was used for $H/D = 2$ case, $r_{lim} = 4.5D$ was used for $H/D = 6$ case (D is the diameter of the nozzle). Both refinement studies were done for the $\varphi - f$ model with a time-scale limiter employed ($C_{lim} = 0.5$). We can see in tables A.1 and A.2 that the solutions lie in the asymptotic range of convergence, since $C \approx 1$. Due to a lack of sufficient computational recourses and a large number of computations conducted, the meshes chosen to compute the presented results were actually not the finest ones, but the coarser ones with the designation "Grid 2".

	Relative grid spacing	Number of cells	$\overline{\dot{q}}$ ($\mathrm{K\,m^{-1}}$)
Grid 1	1	200 334	79 957.5
Grid 2	$\doteq \sqrt{2}$	100 125	80 960.4
Grid 3	$\doteq 2$	50 053	82 595.6

Grid comparison	GCI (%)	
Grid1 - Grid2	1.9385	**p = 1.645**
Grid2 - Grid3	3.3878	**C = 1.0119**

Table A.1: Summary of the grid refinement study for impinging jet $H/D = 2$.

	Relative grid spacing	Number of cells	$\overline{\dot{q}}$ ($\mathrm{K\,m^{-1}}$)
Grid 1	1	220 280	73 509.4
Grid 2	$\doteq \sqrt{2}$	110 109	74 031.1
Grid 3	$\doteq 2$	55 070	75 004.1

Grid comparison	GCI (%)	
Grid1 - Grid2	1.0255	**p = 1.798**
Grid2 - Grid3	1.8992	**C = 1.007**

Table A.2: Summary of the grid refinement study for impinging jet $H/D = 6$.

A.2 2D infinite serpentine

The choice of appropriate parameter with which the author conducted a refinement study was motivated by how the authors of the article [7] defined surface averaged friction velocities for the inner and outer walls of the serpentine:

$$u_{\tau i} = \frac{1}{S_i}\int_{S_i} u_\tau \,\mathrm{dS};\; u_{\tau o} = \frac{1}{S_o}\int_{S_o} u_\tau \,\mathrm{dS}, \tag{A.1}$$

where subscripts "i" denote the inner and "o" outer wall respectively. The author found it easier to compute the means of absolute friction velocities:

$$|u_{\tau i}| = \frac{1}{S_i}\int_{S_i} |u_\tau| \,\mathrm{dS};\; |u_{\tau o}| = \frac{1}{S_o}\int_{S_o} |u_\tau| \,\mathrm{dS}. \tag{A.2}$$

Note that the individual friction velocities in the separation region are negative, but will be added to the total sums in (A.2) as positive values. Then the averaged velocities were combined into a single friction velocity as it was done in the article:

$$|u_\tau| = \sqrt{0.5\,(|u_{\tau i}|^2 + |u_{\tau o}|^2)}.$$

This definition of total surface averaged friction velocity was used in the refinement study. This time, the study was done with the $\varphi - f$ model without any modifications applied.

The results of the study are shown in table A.3. The parameter $|u_\tau|$ seems to have almost reached grid convergence. Authors of the article describing the DNS of infinite serpentine have also done a mesh convergence study and have found out that the results are very sensitive to the mesh refinement in the normal direction of the walls, but much less so to the refinement in the streamwise direction. Thus a preventive measure was taken and the coarsest grid already contained 150 cells with very small cell-to-cell expansion ratio < 1.05 (with values of y_+ still below one). If the coarsest grid wasn't constructed this way, the computed values of GCI could easily rise to > 10 %, as the author experienced firsthand. Again the grid designated as "Grid 2" was used to compute the presented results, for the same reasons as in the case of an impinging jet. The convergence rates were somewhat higher than in the impinging jet, so computing on a grid of 192 000 cells wasn't as time-consuming.

	Relative grid spacing	Number of cells	$\lvert u_\tau \rvert$ (m^2s^{-2})
Grid 1	1	384 000	0.203 084 24
Grid 2	$\sqrt{2}$	192 000	0.203 219 23
Grid 3	2	96 000	0.203 463 21

Grid comparison	GCI (%)	
Grid1 - Grid2	0.1029	**p = 1.707**
Grid2 - Grid3	0.1858	**C = 1.00066**

Table A.3: Summary of the grid refinement study for 2D infinite serpentine.